INVESTIGATION OF ATMOSPHERIC DISPERSION IN AN URBAN ENVIRONMENT

USING SF$_6$ TRACER AND NUMERICAL METHODS

By

JULIA EMILY FLAHERTY

A thesis submitted in partial fulfillment of
the requirements for the degree of
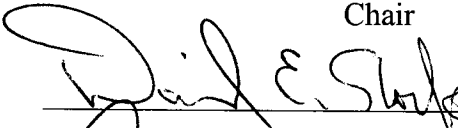
MASTER OF SCIENCE IN ENVIRONMENTAL ENGINEERING

WASHINGTON STATE UNIVERSITY
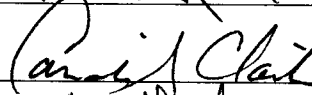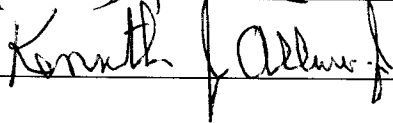Department of Civil and Environmental Engineering

AUGUST 2005

To the Faculty of Washington State University:

The members of the Committee appointed to examine the thesis of JULIA EMILY

FLAHERTY find it satisfactory and recommend that it be accepted.

Chair

INVESTIGATION OF ATMOSPHERIC DISPERSION IN AN URBAN ENVIRONMENT

USING SF$_6$ TRACER AND NUMERICAL METHODS

Abstract

by Julia Emily Flaherty, M.S.
Washington State University
August 2005

Chair: Brian K. Lamb

Pollutant transport and dispersion in urban environments is a complex topic due to the variety of parameters that affect the flow in built-up landscapes. Although the effects of individual parameters are fairly well understood, the interactions among these various factors are still not well known. The goal of this research was to investigate dispersion in an urban environment using a combination of experimental tracer and numerical fluid dynamic methods. First, an extensive field campaign was conducted in Oklahoma City (OKC), Oklahoma during July, 2003 to collect a variety of measurements, including meteorology, turbulence, energy balances, and tracer concentrations related to controlled SF$_6$ tracer releases from locations in the city center. Vertical profiles of tracer concentration measured by Washington State University presented here indicate that the urban landscape is very effective in mixing the plume vertically. As a simple analysis tool for emergency response, a maximum normalized concentration curve has been developed. The curve from the field data predicts higher concentrations than the centerline values predicted by the Guassian plume equation; however, it compared well with results from a computational fluid dynamics analysis.

The second component of this research involved utilizing a computational fluid dynamics code to model a field case from OKC. The many short buildings in this domain had a relatively small effect on the flow field, while the few tall buildings drove the transport and dispersion of tracer gas through the domain. This modeling work indicated that relatively accurate results can be obtained from the k-ε closure model, and that these results can be improved by including the effects of surface heating. The isothermal base case predicted concentrations within 50% of the field measurements, while a convective case with ground and building surfaces 10 deg C hotter than the air temperature improved the modeled profile to within 30% of observations.

TABLE OF CONTENTS

LIST OF TABLES

LIST OF FIGURES

ATTRIBUTION

This thesis is comprised of 4 chapters. Chapter One contains an overview of the research topic. Chapters Two and Three are each independent manuscripts that will be submitted for publication. Finally, Chapter Four provides a summary and conclusions of this research. I am the primary author for the whole of the thesis as well as the manuscripts; however, other individuals have contributed to these papers as described below.

The first paper, entitled "Vertical Tracer Concentration Profiles Measured during the Joint Urban 2003 Dispersion Study and a Maximum Concentration Curve for Emergency Response," will be published under the authorship of Julia Flaherty, Eugene Allwine, Brian Lamb, and Jerry Allwine. Eugene Allwine developed the instrumentation used in this research, and conducted the field campaign with Julia Flaherty. Brian Lamb and Jerry Allwine were instrumental in developing data analysis suggestions as well as editorial comments on the manuscript.

The second paper, which is contained in Chapter Three, is entitled "Using Computational Fluid Dynamics to Model Urban Dispersion." Julia Flaherty, David Stock, and Brian Lamb will publish this work. Flaherty conducted all modeling work under the guidance of Stock and Lamb.

Dedication

To the memory of my mother

CHAPTER ONE

INTRODUCTION

Pollutant transport and dispersion in urban environments is very complex. While open field dispersion is generally governed by atmospheric stability, dispersion in cities is affected by a variety of other issues. Over the past 40 years, researchers have explored field measurement campaigns, physical modeling, and numerical modeling as a means to understand the way air travels and pollutants disperse through urban environments. Building geometry, surface heating, and moisture, among other parameters, have been investigated. The effects of individual parameters are fairly well understood; however, the interactions among these various factors are still not well known.

One of the seminal field campaigns in urban dispersion research was the St. Louis study (McElroy and Pooler, 1968). In this investigation, 42 near-ground releases were conducted, and concentrations were measured from 0.5 to approximately 10 miles from the source. These experiments revealed that both vertical and horizontal dispersion is enhanced over the open field conditions, such as those measured during Project Prairie Grass (Barad, 1958).

There have been numerous investigations of urban environments conducted since the St. Louis experiment. Some of the studies that have been performed in the past decade are outlined here. Grimmond et al. (2004) described turbulence and surface energy balance flux results from a study conducted in the core of Marseille, France during the summer of 2001. This study supplied additional data for understanding stability conditions in cities, and measured increased latent heat and reduced carbon dioxide fluxes due to vegetation in urban environments. Kastner-Klein et al. (2003) demonstrated that traffic-produced turbulence, or TPT, is important in the scaling equations used to compute pollutant concentrations in a street canyon. Indirect validation

of the effect of TPT was performed through wind tunnel modeling as well as field measurements in Germany and Copenhagen.

Additionally, large urban field campaigns with a variety of instrumentation have been deployed in the past few years. BUBBLE, or the Basel UrBan Boundary-Layer Experiment, was unique in that measurements were conducted for a year, from the summer of 2001 to 2002. This was supplemented with a month-long intensive observation period that was conducted between June and July of 2002. Sonic anemometers, wind profilers, lidar, sodar, and other instruments deployed in the urban core, suburban areas, and the rural background provided an excellent dataset for characterizing the urban boundary layer. The DAPPLE experiment (Arnold et al., 2004), on the other hand, concentrated on dispersion processes on a smaller scale: a street canyon intersection in London. This 4-year project has currently conducted two field measurement campaigns that measured meteorology, pollutant levels, tracer concentrations, and personal exposure. Both of these studies have collected large quantities of data, but conclusive results have yet to be presented.

Other field campaigns, conducted in the U.S., include Urban 2000 (Allwine et al., 2002), which was embedded in the VTMX (Vertical Transport and MiXing) program (Doran et al., 2002). This experiment aimed to understand the processes that drive vertical transport and mixing in urban environments and complex terrain during both day- and night-time conditions. These measurements were collected in Salt Lake City, Utah, and were unique in that tracer measurements were conducted over a large range of scales. Tracer concentrations were tracked from its movement around an individual building, through an array of buildings, and out into the surrounding region over a 10-km diameter. Another measurement program, described by Venkatram et al. (2004) was conducted in San Diego, California. This study was supported by

the California Air Resource Board (CARB) to investigate the environmental justice implications of the impact of industries, shipyards, and naval installations on the community of Barrio Logan. The residential area was comprised of generally homogeneous 1-story buildings, and near-surface tracer measurements were conducted on arcs out to 2-km.

A number of studies applying computational fluid dynamics (CFD) to urban flows have also been employed in recent years. Investigation of street canyons lends itself easily to two-dimensional modeling, such as the work of Lien et al. (2004) and Chan et al. (2002). Lien et al. used the standard, Kato-Launder, renormalization group (RNG), and non-linear k-ε models to investigate flow that develops through an array of obstacles and compared results with a wind tunnel study. Chan et al. also utilized a series of k-ε closures (standard, renormalization group, and realizable) to examine the effects of wind speed, source strength, and street canyon configuration in a single street canyon.

Although many groups have utilized 2D domains, field campaigns such as those mentioned above have verified the highly three-dimensional nature of pollutant dispersion. Increasingly sophisticated 3D modeling efforts have also been conducted in the past few years. These also range from many computations with idealized obstacles to a few with true urban landscapes. For example, Hamlyn and Britter (2005) utilized the Reynolds stress model to investigate three different packing densities of a regular array of cubes. This work was validated with both a physical model and a large eddy simulation (LES) numerical model. Calhoun et al. (2004) described measurement and modeling efforts about a single complex building. This simulation was performed for several wind directions and accounted for trees near the building as momentum sinks. Although vortices were occasionally shifted in space, the average dynamics of the flow was captured well.

The goal of this research was to investigate dispersion in an urban environment using a combination of experimental tracer and numerical fluid dynamic methods. This is accomplished through the two independent manuscripts presented in this thesis. First, an extensive field campaign was conducted in Oklahoma City, Oklahoma to collect a variety of measurements over a relatively large spatial extent. Secondly, a computational fluid dynamics model was used to simulate a 10-minute field case and to investigate the mechanisms for dispersion in the urban landscape.

Chapter two describes some results from Joint Urban 2003, which was conducted in June and July of 2003 and involved over 20 principal investigators and 150 researchers. The main goal of this field study was to develop a high-quality dataset of meteorology on a 24-hr basis throughout the city, complemented by concentration data from 10 tracer release periods. In addition to the scientific question concerning pollutant transport and dispersion through urban landscapes, this field campaign also aimed to collect data to develop tools to aid in homeland security efforts.

A variety of tracer analyzers and samplers were deployed, from the source region out to a 4-km arc. A unique contribution from Washington State University was a vertical tracer profile system, called Travert, which was erected approximately 1-km from the release position. Simultaneous 5-minute averages of SF_6 tracer concentrations were measured at seven levels, from 10 to 75 meters above the ground. The complete set of profile data collected during this campaign is presented in the Appendix as Figures A-1 through A-10.

Chapter three details a numerical analysis of one of the field cases conducted during the Joint Urban 2003 field campaign. The Navier-Stokes equations exactly define fluid flow; however, it is impossible to solve these equations for turbulent flow due to the scales of motion

4

that must be resolved. Launder and Spalding (1972) described this as a problem in computing power. For proper computation of turbulent flow, the smallest scales of dissipation must be resolved. The size of these smallest scales in gaseous flows is about 0.1mm, and if there were 10^5 discrete points in the domain, it would only cover a cubic centimeter of space. Launder and Spalding indicate that this would be a challenge for even the most sophisticated computers. The advanced parallel computers of today are far more powerful than computers of the 1970s; nonetheless, it is still impossible to cover city-scale flow with 0.1 mm resolution. Current studies using direct numerical simulation (DNS) of the Navier-Stokes equations typically utilize about 512^3 cells.

Most of the measurements, including those from the vertical profile system, in the Joint Urban campaign were time-averaged concentrations of a tracer gas. Therefore, it was appropriate to consider Reynolds Averaged Navier-Stokes (RANS) modeling to explore the field case. However, Reynolds averaging the Navier Stokes equation results in additional unknowns that must be modeled. In this case, the standard k-ε closure model was utilized, as it is a relatively simple model with respectably accurate results.

REFERENCES

Allwine, K. J., J.H. Shinn, G.E. Streit, K.L Clawson, and M. Brown, 2002: Overview of Urban 2000: A multiscale field study of dispersion through an urban environment. *Bull. Amer. Meteor. Soc.,* **83 (4)**, 521-536.

Arnold, S.J., H. ApSimon, J. Barlow, S. Belcher, M. Bell, J. W. Boddy, R. Britter, H. Cheng, R. Clark, R. N. Colvile, S. Dimitroulopoulou, A. Dobre, B. Greally, S. Kaur, A. Knights, T. Lawton, A. Makepeace, D. Martin, M. Neophytou, S. Neville, M. Nieuwenhuijsen, G. Nickless, C. Price, A. Robins, D. Shallcross, P. Simmonds, R.J. Smalley, J. Tate, A.S. Tomlin, H. Wang, and P. Walsh, 2004: Introduction to the DAPPLE Air Pollution Project, *Science of The Total Environ.*, **332**, 139-153.

Barad, M.L., 1958: Project Prairie Grass, A Field program in diffusion. Geophys. Res. Paper, **59** Vols. I and II, Air Force Cambridge Reseach Center, Bedford, MA.

Calhoun, R., F. Gouveia, J. Shinn, S. Chan, D. Stevens, R. Lee, and J. Leone, 2004: Flow around a complex building: comparison between experiments and a Reynolds-averaged Navier-Stokes approach. *J. Appl. Meteor.*, **43**, 696-710.

Chan, T.L., G. Dong, C.W. Leung, C.S. Cheung, and W.T. Hung, 2002. Validation of a two-dimensional pollutant dispersion model in an isolated street canyon. *Atmos. Environ.*, **36**, 861-872.

Doran, J.C., J. D. Fast and J. Horel. 2002: The VTMX 2000 campaign. *Bull. Amer. Meteor. Soc.* **83 (4)**, 537–551.

Hamlyn, D., and R. Britter, 2005: A numerical study of the flow field and exchange processes within a canopy of urban-type roughness. *Atmos. Environ.*, **39**, 3243-3254.

Kastner-Klein, P., E. Fedorovich, M. Ketzel, R. Berkowicz, and R. Britter, 2003: The modeling of turbulence from traffic in urban dispersion models – Part II: Evaluation against laboratory and full-scale concentration measurements in street canyons. *Env. Fluid Mech.*, **3**, 145-172.

Launder, B.E., and D.B. Spalding, 1972. Lectures in mathematical models of turbulence. Academic Press, London, England.

Lien, F.S., E. Yee, and Y. Cheng, 2004: Simulation of mean flow and turbulence over a 2D building array using high-resolution CFD and a distributed drag force approach. *J. Wind Eng. & Ind. Aerodyn.*, **92,** 117-158.

McElroy, J.L., and F. Pooler, 1968: St. Louis Dispersion Study Volume 1 & 2. National Air Pollution Control Administration. U.S. Department of Health, Education, and Welfare, Durham, N.C.

Rotach, M.W., R. Vogt, C. Bernhofer, E. Batchvarova, A. Christen, A. Clappier, B. Feddersen, S.-E. Gryning, G. Martucci, H. Mayer, V. Mitev, T.R. Oke, E. Parlow, H. Richner, M. Roth, Y.-A. Roulet, D. Ruffieux, J.A. Salmond, M. Schatzmann, and J.A. Voogt, 2005: BUBBLE – an urban boundary layer meteorology project. *Theor. Appl. Climatol,.* [Avail online at http://www.springerlink.com/openurl.asp?genre=article&id=doi:10.1007/s00704-004-0117-9]

Venkatram, A., V. Isakov, D. Pankratz, J. Heumann, and J. Yuan, 2004: The analysis of data from an urban dispersion experiment. *Atmos. Environ.*, **38**, 3647-3659.

CHAPTER TWO

VERTICAL TRACER CONCENTRATION PROFILES MEASURED DURING THE JOINT URBAN 2003 DISPERSION STUDY AND A MAXIMUM CONCENTRATION CURVE FOR EMERGENCY RESPONSE

Julia Flaherty, Eugene Allwine, and Brian Lamb

Laboratory for Atmospheric Research, Department of Civil and Environmental Engineering,

Washington State University, Pullman, WA 99164

K. Jerry Allwine

Pacific Northwest National Laboratory, Richland, WA 99352

ABSTRACT

An atmospheric tracer dispersion study known as Joint Urban 2003 was conducted in Oklahoma City, Oklahoma during the summer of 2003. As part of this field program, vertical concentration profiles were measured at approximately 1 km from downtown tracer gas release locations. These profiles indicated that the urban landscape is very effective in mixing the plume vertically. The plume centerline (as determined by the maximum concentration over the 65-meter depth of measurements) can occur at any vertical position. The concentration observed at a given downwind receptor is predominantly dependent on the wind direction. As a simple analysis tool for emergency response, a maximum normalized concentration curve was developed with 5-minute averaged measurements. These curves give the maximum concentration (normalized by the release rate) that would be observed as a function of downwind distance in an urban area. The 5-min data resulted in greater concentrations than the Gaussian plume equation predicts. However, the curve compared well with data from a CFD analysis. This dispersion dataset is a valuable asset not only for refining air quality models, but also for developing new tools for emergency response personnel in the event of a toxic release.

1. Introduction

Atmospheric transport and dispersion studies have been vital in the development and evaluation of air quality models. Early experiments, such as Project Prairie Grass (Barad, 1958) and the Wangara Experiment (Clarke et al., 1971) were fundamental to the study of plume dispersion. High quality datasets such as those produced from these principal experiments

continue to be referenced as a source of analysis and validation data. Some examples include Draxler's 1976 work and van Ulden's 1978 work on diffusion coefficients as well as recent improvements to these diffusion parameters by Britter et al. (2003). Draxler presents an excellent summary of early diffusion experiments in his chapter of Atmospheric Science and Power Production (1984).

Many of these early atmospheric studies were conducted under relatively simple dispersion conditions. As Molina and Molina (2004) and Gurjar and Lelieveld (2005) point out, nearly half of the world's population now lives in urban areas. Creating models that are more applicable for the urban landscape has increasingly become a research priority. Many people are exposed to a variety of urban pollutants daily; however, we still have an incomplete understanding of urban pollutant transport and dispersion. Britter and Hanna (2003) highlighted research that has investigated various components of urban flow. They pointed out that although we have a fairly good understanding of the individual processes that take place in urban landscapes, how these processes combine and interact with one another is less clear.

In recent work, field studies, wind tunnel experiments, and numerical models have been used to investigate dispersion around individual buildings (e.g., Calhoun et al., 2004, Meroney et al., 1999), in single street canyons (e.g., Caton et al., 2003; Sagrado et al., 2002), and through small multi-building industrial and urban areas (e.g., Guenther et al., 1990; Scaperdas and Colvile, 1999). Additionally, large-scale dispersion studies have been performed for more complex settings. These include DAPPLE in London (Arnold et al., 2004), which studied a street canyon intersection as a potential hot-spot for personal exposure, BUBBLE, conducted in Basel, Switzerland (Rotach et al., 2004), which investigated dispersion over a fairly regular array of buildings, Urban 2000 in Salt Lake City, Utah (Allwine et al., 2002), which investigated the

homeland security implications of an atmospheric release in an urban area, and the Barrio Logan study in San Diego (Venkatram et al., 2004), which was an environmental justice case that looked at transport of emissions from an industrial area to a residential area 2 km downwind. This paper will discuss some results from another urban dispersion study, Joint Urban 2003 (JU03), which was conducted in Oklahoma City, Oklahoma.

The goal of this field study was to build a high-quality, comprehensive urban dispersion dataset to fill in the gaps in our understanding of these complex flows. The data is available for the characterization of urban flow and scalar dispersion as well as for the evaluation, modification, and improvement of dispersion models. This is important for accurate prediction of urban air quality as well as for determining the impact of accidental or intentional biochemical releases.

In this study, over 20 principal investigators and 150 researchers collected meteorological and tracer data throughout Oklahoma City. The month-long field program included 10 intensive operating periods, or IOPs. Each IOP was eight hours long, and consisted of three 30-minute continuous sulfur hexafluoride (SF_6) tracer releases and four instantaneous puff releases. Tracer releases were conducted at a height of approximately 2 meters above ground level, and release rates were typically on the order of 3 g s^{-1} during the continuous releases and 500 g during puffs. The 10 IOP dates were selected based on predicted wind directions from the south or southeast. Three different release locations were utilized in order to maximize the data collected by the array of downwind receptors. Six of the releases occurred during the day, while four were conducted during the night. In addition to the 10 IOPs, an additional "Mini" IOP was conducted. In this case, the wind direction was not appropriate to conduct a complete IOP, so a new release position was selected about five blocks upwind of the profile site. Several sonic anemometers

and tracer analyzers were employed in addition to the instrumentation on the 90-m profile system.

During each tracer release, tracer measurement instruments were positioned on sampling arcs at one-, two- and four-km from the central business district (CBD) of Oklahoma City (OKC), as well as in the street canyons nears the release position. Tracer concentrations were measured using a variety of instrumentation, including bag samplers, real-time infrared analyzers, and real-time electron capture detector (ECD) analyzers. Additionally, a dense grid of sonic anemometers, sodars, lidars, radiosondes, tethersondes, and radio acoustic sounding systems made meteorological measurements throughout the city on a 24-hr basis for the duration of the campaign.

The objective of this paper is to present vertical concentration profile data collected using Travert – a novel automated profile sampling system. Additionally, a simple maximum concentration analysis utilizing the various tracer data collected during this campaign is discussed. Section 2 of this paper briefly describes the experiment site, while section 3 discusses the wind and tracer instruments on the vertical profile system. Section 4 is devoted to a description of these data. Section 5 demonstrates the use of simple normalized maximum concentration curves as a preliminary planning tool. Finally, conclusions are presented in section 6.

2. Site description

Oklahoma City is situated in the middle of the state of Oklahoma on the flat terrain and grasslands of the Great Plains. During the summer, winds in OKC are generally from the south

and the average wind speed for the month of July is 5.1 m s^{-1}. July is OKC's warmest month, with a mean temperature of about 28°C (82°F). The mean daily maximum temperature during this month is 34°C (93.4^{o}F), while the mean daily minimum is 21.4^{o}C (70.6^{o}F) (NWS, 2003). As mentioned in the previous section, tracer measurements were made during the hottest part of the day, when convection plays a large role, as well as during the coolest part of the night.

Oklahoma City has a population of approximately 500,000 people, with 1,180,000 within the metropolitan area (Census 2000). This dispersion study was conducted in the heart of downtown OKC, which contains all of the tallest buildings in the city as well as many shorter buildings of various shapes. The tallest building in the city is the Bank One building, which is about 150 meters tall. The central business district contains two other buildings that are at least 120 m tall, and eight additional buildings that are between 75 m and 120 m tall. Other buildings in downtown Oklahoma City tend to be less than 50 m, with many structures about 15 m tall. Figure 2-1 shows the urban landscape. This range of building dimensions, although rather complex to model accurately, is characteristic of many "medium-sized" U.S. cities.

The role of the Washington State University (WSU) Laboratory for Atmospheric Research (LAR) was in the measurement of tracer concentrations at a 90-m wind speed and tracer concentration vertical profile system erected approximately one-km from the downtown release points. The circular markers on Figure 2-1 indicates the locations of the tracer release points, while the profile site is denoted by a triangular marker. This site was on the southwest corner of the intersection of 8th and Harvey. Other obstacles that are not depicted in Figure 2-1 that had a relatively minor effect on the measurements made at this crane site include several shipping containers and trailers located on the southern half of the block occupied by the crane measurement system.

3. Profile system

a. Instrumentation

A ladder structure with two vertical cables in tension and eight horizontal crossbars was utilized to support the vertical profile system. A large crane, about 90 meters tall, suspended this ladder system while a smaller crane served to anchor it. This crane was instrumented with sonic anemometers on each of the eight crossbars. Researchers from Lawrence Livermore National Laboratory (LLNL) collected sonic anemometer data continuously throughout the month-long study. During intensive operating periods, sequential five-minute averaged concentrations of SF_6 tracer gas were measured simultaneously at seven heights, from about 10 to 75 meters above ground level. These inlets were mounted on the western guide cable as depicted in Figure 2-2. (See Table 2-1 for the heights of the instrumentation on the crane.) The ladder system was quite stable; however, in high winds, it appeared that it moved laterally. Fortunately, there was little torsional movement in the system, and time averaging minimized the effects of lateral movements.

The WSU Travert system allows for automated collection and analysis of five-minute average samples. In operation, air is drawn through seven 91.4-meter (300-feet) long polyethylene sample lines to the instrument. It is equipped with 14 10-L Tedlar® bags, so while one set of seven bags are collecting air samples, the second set of bags are sequentially analyzed. The SF_6 concentration in a single bag was determined by drawing air from the bag to the analyzer for 30 seconds. Between the sample analysis and collection, the Tedlar bags were evacuated completely to ensure that the bags were "clean" for the next sampling period.

13

Subsequently, the bag was evacuated until the beginning of the sample collection cycle. Laboratory tests indicated that the bags did not require a flushing cycle.

The Travert also included an on-line calibration by incorporating a zero air and SF_6 span gas into each five-minute analysis cycle. Calibration gases were sampled for 45 seconds each. The span gases utilized during the IOPs were either 527 parts per trillion by volume (ppt) or 4950 ppt (Scott-Marin, Inc., ±5% certified accuracy).

The analyzer was a modified Hewlett-Packard gas chromatograph equipped with an electron capture detector (ECD) that sequentially analyzed the bags. This first involved combining the air with H_2, then passing it through a packed bed of palladium catalyst. This converted the O_2 in the air to H_2O. Next, the air was passed through a nafion tube with a counter-current flow of N_2. This removed the H_2O from the sample stream. The sample stream was then passed to the ECD, where the voltage changes due to the SF_6 in the stream provided the signal for concentration. See Benner and Lamb (1985) for additional information about this type of detector system.

The final component of this system was the computer, which ran a Labview program that regulated the pumps to ensure that samples were collected in the appropriate bags and that the samples were pumped to the detector in the correct sequence. The program was also responsible for collecting the 1-Hz signal from the ECD and writing the data files. See Figure 2-3 for a photo of the profile system.

b. Measurement system characteristics

The lag time, or the time for the sample to travel down the tubing to the Travert system, was calculated using the measured flow rate (approximately 101 standard L min^{-1}), cross-

sectional area of the polyethylene tubing (6.35 mm, or ¼-inch, inner diameter), and its length. Although the inlet tubes were mounted at different heights, they all had equal lengths of tubing for equal sample travel times. The lag time was approximately 12 seconds throughout the test periods. This is a small fraction of the five-min sampling time, and is therefore neglected in the data analysis.

The lower detection limit for the ECD was determined as three times the noise of the instrument. Table 2-2 presents the lower detection limits obtained from this method for each of the intensive operating periods. Additionally, factors such as the duration since the tracer release, comparisons between concentrations at different profile levels, and the winds at the different levels were considered when determining whether a low concentration was valid.

Actual calibration coefficients utilized in the post-processing of these data were determined with several factors in mind. A suite of calibration gases was analyzed with this system during non-IOP periods. By considering an average response for calibration runs that were conducted on the non-IOP periods as well as the span checks that were run during each 5-minute analysis cycle, an appropriate calibration factor was applied. Furthermore, when applying the calibration to the raw voltage data that was collected from the ECD, the zero air voltage that was subtracted from the sample response was the linearly interpolated zero between the current and previous analysis period to account for short-term instrument drift.

There were several sources of error in the measurement of tracer concentrations. First, there was a systematic error (±5%) associated with the concentration of the standard gas utilized for the calibration of the voltage signal from the ECD. Additionally, there was a random error from the instrument itself. This was quantified by determining the coefficient of variability (CV) of the span gas measurement. The coefficient of variability was calculated as the ratio of the

standard deviation of the signal to the mean signal, and was expressed as a percent. Table 2-3

lists the errors associated with the final reported SF_6 concentration for each study day. The

typical error during this study was ±8%.

4. Tracer profile data

This field experiment included a total of 32 continuous releases of SF_6 tracer during the

11 IOPs. The meteorological conditions during these release periods were quite favorable, and

26 of these releases resulted in a hit (detectable SF_6 concentration) at the profile site. Table 2-4

presents a summary of the date, time, release position, and average wind speed, wind direction

and the distance from the source to the crane site for each IOP. Vertical profiles and time series

graphs of the data collected during this campaign are presented in this section.

The vertical profiles collected from this site show that tracer was relatively well mixed

through the depth of the measurements, and that most of the variation in tracer concentration

observed in the profile time series were related to changes in wind direction as opposed to

changes in turbulence. Figure 2-4 presents profiles from four different IOPs. These profiles

have shapes that are representative of the profiles observed at this site during the 30-minute

continuous SF_6 releases. Generally, near-surface concentrations were not significantly higher

than concentrations at greater heights. Additionally, over the entire study, the lowest

concentration measured along the vertical profile was typically within 50% of the maximum

concentration. The standard Gaussian concentration profile that might be expected in an open

field was not observed in this urban environment due to the mixing generated by the urban

landscape. Although the depth of tracer measurements made in a street canyon in Basel,

Switzerland (Rotach et al., 2004) was only about 14 meters compared to the 65-meter depth of measurements made in this study, results from both experiments indicate very low gradients in the vertical tracer concentration profile. Both studies were conducted in flows with high convective and mechanical mixing.

Another feature to note from these figures is that there is no "typical" profile shape for this particular site, or even a particular hour. Of the three plots, Figure 2-4 (c) exhibits the most consistent shape in the 5-minute profiles over this hour of data. The general shape of the concentration profile was similar over the hour and near-surface concentrations were slightly higher than the upper receptors. However, profiles in Figure 2-4 (a) exhibit a significant degree of variability. The position of the maximum concentration observed in any five-min period varied everywhere along the profile.

Figure 2-5 shows vertical tracer concentration profiles from two of the 20-minute continuous releases conducted during the Mini IOP. Concentrations from these periods are higher than those shown in Figure 2-6 not only because the release rate was greater, but also because the release position was much closer to the crane site. Another contrast to the previous figure is the distinct slope in the tracer profile. At 1245, the topmost concentration was less than half of the 11-meter sample, and at 1235, the 76-meter receptor measured a tracer concentration that was a quarter of the 11-meter sample. The differences in the profiles shown in Figures 2-4 and 2-5 may be attributable not only to differences in the distance that the plume travels, but also in the mean height of the buildings between the source and receptor. Many of the buildings in the CBD were between 70 and 120 meters tall, whereas there was only one building of significant height between the Mini release location and the crane. During this IOP, the tallest building was about 70 meters tall, and the typical building height was less than 8 meters.

17

Additionally, the concentration profile shapes can be explored through the profiles of meteorology. Figure 2-6 shows wind speed, wind direction, and turbulent kinetic energy profiles from the crane site during the continuous releases presented in Figure 2-5. Note that these sonic anemometer data are 10-minute averages, with the time stamp representing the beginning of the measurement period. The timestamps for the five-minute average tracer concentrations, on the other hand, represent the end of the sampling period. Profiles of meteorology tended to be fairly consistent over this hour. Their shapes were quite similar between periods, and their range of values was small. The wind direction was nearly uniform above 15 meters, with a 10- to 15-degree shift to the south for the lowest two anemometers. The 1210 CDT meteorology period appears to be somewhat of an outlier compared to the other profiles in this hour, and correspondingly, the 1215 CDT and 1220 CDT tracer concentration profiles appeared to have low values as well as a small gradient.

Figure 2-7 presents a summary of normalized tracer concentration data collected during each of the continuous tracer release periods. The concentrations (μg m^{-3}) were normalized by the release rate (in μg s^{-1}). Only the highest concentration observed over the seven inlets is plotted here. Previous figures have shown that there is very little variation in concentration values over the depth of this profile. Note that this figure contains ten panels, and that intensive operating period number seven was omitted from this figure. The meteorology during that study period was not favorable for a plume hit at the crane site, and very little data were collected on this date. Also note that the range of the y-axes for each of the figures are identical, except in the case of the Mini IOP, which had significantly higher observed concentrations compared to the other intensive operating periods. These figures also include a line representing the release rate

with time to indicate the relationship between the release start and end times with the observation of tracer at the receptor.

First, note the range of concentrations observed at the crane site across the various IOPs as well as within each IOP. Although the release positions were slightly different for some of the IOPs, the large differences in observed SF_6 concentration at this receptor were mainly a result of varying meteorology. This range of observed concentrations compares well with the urban data from Barrio Logan reported by Venkatram et al. (2004). Concentrations at 1000 m downwind of their release position were generally between 1 x 10^{-3} to 1 x 10^{-4} s m^{-3}. Although the urban landscape in the Barrio Logan study was more uniform and shorter than OKC, the results from these two studies indicate that at least the order of magnitude is readily predictable.

Each release during JU03 generally exhibited a Gaussian shape with time. For most of the continuous releases, SF_6 tracer was observed in the five-minute period immediately following the beginning of the release, and tracer levels return to background levels within five minutes of the tracer shut-off. For a 4 m s^{-1} wind speed, the approximately 1-km distance between the source and receptor would take about four minutes, so the travel time observed at the crane site matches well with this crude approximation.

Figure 2-8 presents wind speed, wind direction, and turbulent kinetic energy from the crane site during the continuous tracer releases for IOP 5, IOP 8, and the Mini IOP, or Day of Year (DOY) 194, 205, and 196, respectively. The curves represent the 10-minute averaged value of a mid-level sonic anemometer (42.5 meters AGL), while the error bars denote the range of values observed over the depth of the eight sonic anemometers (7.8 to 83.2 meters AGL). The horizontal lines on the wind direction plots represent the straight-line direction to connect the release point with the receptor.

19

The meteorology during Day 194 was the most variable of the three days shown here. Correspondingly, this day also had the greatest fluctuation in measured concentrations. The second release had essentially no observed plume at the crane site, which appears to be due to both a slightly elevated wind speed, which dilutes the plume, and a wind direction that is 30 degrees west of the ideal direction. Day 205 and 196 both had fairly constant meteorological conditions as well as similar plume concentrations between each of the three tracer releases.

Although the previous figure indicates that wind direction may be the main parameter that determines high concentrations at the crane site, scatter plots comparing meteorology with concentration shows this correlation more clearly. Figure 2-9 presents plots of wind speed, the difference between the ideal and observed wind direction, and the square root of the turbulent kinetic energy divided by the wind speed, which is a measure of turbulent intensity. The wind speed, wind direction, and turbulent kinetic energy values were taken from the 42.5-meter sonic anemometer from the crane site. Additionally, only data from the main IOPs were used for this figure.

First, these plots show that the highest concentrations were observed during the nighttime study periods. The maximum daytime measurement was roughly half of the maximum nighttime value. There was no distinct relationship between wind speed and concentration. The highest concentrations occur in the 3- to 5-m s^{-1} range, but were distributed randomly. The wind direction, however, appears to play a major role in the concentrations observed at the crane site. Wind directions that were within about ±20 degrees of the ideal wind direction had the highest

concentrations. Finally, concentrations did not appear to be correlated with the analog of turbulent intensity. There was a relatively small range in values of the turbulent intensity compared to a large range in concentration.

5. Tracer data analysis

As a first step in analyzing the total set of tracer data collected during this campaign, normalized maximum concentrations as a function of downwind distance were investigated. The concept for this analysis was based on the minimum dilution work of Wilson and Lamb (1994) where curves that bounded the observed dilution values were plotted as a function of normalized distance from the release. In the present investigation similar dilution curves were developed utilizing much of the tracer data collected during JU03. These curves were developed without regard to wind direction or wind speed. For practical purposes, this was advantageous in that it can be readily applied in real-life situations when a wind speed and wind direction analysis is not feasible. An exponential curve was fit to the maximum observed concentrations to give an approximation of the radius of impact from a release. This type of information is useful in that, within minutes of a hazardous release, it can provide general guidance about the extent to which the impact will be felt. Although complex computational fluid dynamics modeling and even simplified Gaussian plume modeling may produce more refined results, they are generated at the expense of valuable time. For more immediate information to aid in the response phase of a hazardous release, maximum concentration curves can be used.

Tracer data from the NOAA Air Resources Laboratory Field Research Division (ARLFRD), Volpe, and WSU were used for this analysis. Bag samples collected by ARLFRD and Volpe had a variety of averaging periods, but the 5-minute averaged samples were considered because it was consistent with the WSU crane data. ARLFRD utilized their PIGS

(programmable integrating gas samplers) and Super PIGS, while Volpe used MiniVols manufactured by AirMetrics to collect samples.

Figure 2-10 (a) shows the piecewise maximum concentration curve for 5-minute averaged tracer measurements from the continuous releases. Observed concentrations were normalized by the release rate and plotted as a function of the string distance. The string distance is the length of an imaginary string pulled taut from the release position to the receptor. This is the traveling distance between two points that accounts for an obstacle in between them. For receptors within the CBD, the string distance was measured directly with a map that showed the buildings, such as the one given in Figure 2-1. For receptors outside the central business district, the string distance was simply calculated as 110% of the linear distance between two coordinates.

Using the curve developed in Figure 2-10 (a), a 10-fold reduction in the concentration near the source requires about 75 meters. A city block in Oklahoma City is about 150 meters wide, so individuals only a block further from the source will observe average concentrations that are two orders of magnitude lower. Beyond the first block from the release location, however, the slope of the maximum concentration curve is much more shallow, and about 450 meters is required for a 10-fold reduction in concentration.

The change in slope that occurs at about 120 meters, or approximately 4 urban canopy heights ($4H_u$), can be attributable to differences in the mechanisms for mixing. Within the first 4 canopy heights, individual buildings tend to be important, causing channeling of the plume as well as increased mixing due to recirculation zones and chimney effects. However, as the plume spreads with downwind distance and becomes much larger than the height of the canopy, these building effects become less important. Thus, the break in the curve at approximately 4Hu may

be due to a change in the mechanisms causing plume dilution related to the relative size of the plume and urban structures.

In addition to the maximum concentration curve developed with the 5-min field data, Figure 2-10 (b) shows an analogous curve developed from a computational fluid dynamics analysis, which is described in detail in Chapter Three. The CFD study was conducted with a 10-minute averaging period to model the Mini IOP release. Also, instead of string distances, the concentrations are plotted against the component of the distance along the mean wind direction. This results from the fact that cross-plume lines with constant y-coordinate were used to extract the concentration data from the CFD results. The curves in Figures 2-10 (a) and (b) are very similar, with the sharp slope in the first 170 meters and the intercept replicated well. The breakpoint between the two parts of the piecewise fit is slightly different between the field and CFD data. This is due in part to the particular curve fit that was used in each case, as well as differences in the geometry of the two datasets. The buildings in the CFD study were generally below 10 meters in height; however, a single 70-m tall building was also in the path of the plume.

For comparison, centerline concentrations from the simple Gaussian plume equation, assuming ground-level source and receptors, is presented in Figure 2-11. The curve labeled "Field Sigmas" was computed with typical wind speed and turbulence with data from the 42.5-meter level on the LLNL/WSU profile system. The two broken lines have been computed with the Pasquill-Gifford Turner equations for approximating diffusion coefficients in urban environments. Stability classes B and D are presented simply as an indication of the range of predicted values based on atmospheric stability. Finally, the curve developed in Figure 2-10 (a) is labeled as "5-min fit." While the concentration at the source as predicted by the "5-min fit"

curve is about 20 s m^{-3}, the Gaussian curves predict concentrations that are about 2 orders of magnitude smaller. Near the source, the slopes of the Gaussian curves are steeper than that of the curve developed using the field data. However, by a downwind distance of 120 meters, the "5-min fit" curve is nearly parallel to the Gaussian plume equations. This indicates that when the plume is much wider than the canopy, the geometry of the city is less important and dispersion occurs in a Gaussian manner. The maximum concentrations measured in the field were between two and three orders of magnitude greater than the concentrations predicted by the centerline Gaussian plume equation.

Maximum concentration curves with exposure limit information can be a valuable tool for emergency response personnel. These individuals will have to estimate the type, such as continuous versus instantaneous release and possibly chemical composition, as well as the amount of the release, but will be able to react quickly to make decisions about areas that require shelter in place versus evacuation. Finally, these curves were developed with the data available from the Oklahoma City dispersion experiment, and cities with different urban landscapes may have different plume dispersion characteristics. However, every method that is utilized for emergency response will have its own set of strengths and weaknesses. The advantage of having rapid guidance in the moments following a hazardous release may outweigh the uncertainties of this method.

6. Conclusions

This paper discussed results of the Joint Urban 2003 atmospheric dispersion study. Wind speeds were relatively high throughout the study, and tracer concentrations one kilometer from

the release were detected within five minutes of the start of a tracer release. The urban environment is a very complex landscape, and sometimes counter-intuitive correlations exist between the meteorology and the tracer behavior. Many times, the straight-line transport wind direction will result in the highest concentrations; however, channeling in the street canyons can cause the same wind direction to result in lower concentrations.

Vertical tracer concentration profiles that were collected at the WSU/LLNL crane site show that the plume was mixed well vertically. The meteorology profiles were relatively constant with height over the 75-meter depth of measurements, which implies that the mean gradients are not the mechanism for vertical mixing. Instead, localized phenomena such as chimney effects near buildings or convection due to differential heating may contribute to the low-gradient concentration profiles measured at the LLNL/WSU crane site. These processes can be explored further with computational fluid dynamics modeling.

A maximum concentration curve as a function of downwind distance was developed using 5-minute averaged tracer data from several groups and validated with results from a computational fluid dynamics analysis. The slope of the maximum fit curve for the five-minute data was shallower than the curves predicted by the Gaussian plume equation in the first 200 meters from the source, and parallel to the Gaussian curve for distances greater than 200 meters. Concentrations observed in the field were greater than the predictions from the Gaussian plume equation. Data with different averaging times will be studied in the future to determine a relationship between the maximum five-min concentration and longer or shorter averaging periods. This is important for determining health effects when exposure limits are given for different durations. For certain hazardous compounds, it may be necessary to ensure that a particular dose is not exceeded as opposed to exposure to an instantaneous concentration.

25

The information gained from this study continues to improve our understanding of the mechanisms by which air pollutants disperse through an urban landscape. The OKC dispersion dataset is a valuable asset not only for refining air quality models, but it also for developing additional tools for emergency response personnel in the event of a toxic release.

7. Acknowledgements

REFERENCES

Allwine, K. J., J.H. Shinn, G.E. Streit, K.L Clawson, and M. Brown, 2002: Overview of Urban 2000: A multiscale field study of dispersion through an urban environment. *Bull. Amer. Meteor. Soc.*, **83 (4)**, 521-536.

Arnold, S.J., H. ApSimon, J. Barlow, S. Belcher, M. Bell, J.W. Boddy, R. Britter, H. Cheng, R. Clark, R.N. Colvile, S. Dimitroulopoulou, A. Dobre, B. Greally, S. Kaur, A. Knights, T. Lawton, A. Makepeace, D. Martin, M. Neophytou, S. Neville, M. Niewenjuijsen, G. Nickless, C. Price, A. Robins, D. Shallcross, P. Simmonds, R.J. Smalley, J. Tate, A.S. Tomlin, H. Wang, and P. Walsh, 2004: Introduction to the DAPPLE air pollution project. *Science of the Total Environ.*, **332**, 139-153.

Barad, M.L., 1958: Project Prairie Grass, A Field program in diffusion. Geophys. Res. Paper,
    59 Vols. I and II, Air Force Cambridge Reseach Center, Bedford, MA.

Benner, R. L., and B. Lamb, 1985: A fast response continuous analyzer for halogenated
    atmospheric tracers. *J. Atmos. and Oceanic Tech.,* **2 (4)**, 582-589.

Britter, R.E., and S.R. Hanna, 2003: Flow and dispersion in urban areas. *Annu. Rev. Fluid
    Mech.*, **35**, 469-496.

Britter, R. E., S.R. Hanna, G.A. Briggs, and A. Robins, 2003: Short-range vertical dispersion
    from a ground level source in a turbulent boundary layer. *Atmos. Environ.*, **37**, 3885-3894.

Calhoun, R., F. Gouveia, J. Shinn, S. Chan, D. Stevens, R. Lee, and J. Leone, 2004: Flow
    around a complex building: Comparison between experiments and a Reynolds-averaged
    Navier-Stokes approach. *J. Appl. Meteor.*, **43**, 696-710.

Caton, F., R.E. Britter, and S. Dalziel, 2003: Dispersion mechanisms in a street canyon. *Atmos.
    Environ.*, **37**, 693-702.

CENSUS cited 2000. American FactFinder. [available on-line at
    http://factfinder.census.gov/home/saff/main.html]

Clarke, R.H., A.J. Dyer, R.R. Brook, D.G. Reid, and A.J. Troup, 1971: The Wangara
    Experiment: Boundary layer data. *Div. of Meteor. Phys. Tech Paper No* 19. CSIRO,
    Melborne.

Cowan, I.R., I.P. Castro, and A.G. Robins, 1997: Numerical considerations for simulations of
    flow and dispersion around buildings. *J. Wind Eng. & Ind. Aerodyn.,* **67 & 68**, 535-545.

Draxler, R.R., 1976: Determination of atmospheric diffusion parameters. *Atmos. Environ.*, **10**,
    99-105.

Draxler, R.R., 1984: Diffusion and Transport Experiments. *Atmospheric Science and Power
    Production*, D. Randerson, Ed., Technical Information Center Office of Scientific and
    Technical Information, United States Department of Energy, 367-422.

Guenther, A., B. Lamb, and E. Allwine, 1990: Building wake dispersion at an Arctic industrial
    site: field tracer observations and plume model evaluations. *Atmos. Environ.*, **24A** (9), 2329-
    2347.

Gurjar, B.R., and J. Lelieveld, 2005: New Directions: Megacities and global change. *Atmos.
    Environ.,* **39**, 391-393.

Hosker, Jr., R.P., 1984: Flow and dispersion near obstacles. Atmospheric Science and Power
    Production. Darryl Randerson, Ed., Technical Information Center, DOE, 241-326.

Lien, F., and E. Yee, 2004: Numerical modeling of the turbulent flow developing within and over a 3-D building array, Part I: A high-resolution Reynolds-averaged Navier-Stokes approach. *Boundary-Layer Meteor.,* **112**, 427-466.

Meroney, R.N., B.M. Leitl, S. Rafailidis, and M. Schatzmann, 1999: Wind-tunnel and numerical modeling of flow and dispersion about several building shapes. *J. Wind Eng. & Ind. Aerodyn.,* **81**, 333-345.

Molina, M.J., and L.T. Molina, 2004: Megacities and atmospheric pollution. *J. Air & Waste Manage. Assoc.*, **54**, 644-680.

NWS, cited 2003: Preliminary local climatological data. [Available online at http://www.srh.noaa.gov/oun/climate/get_f6.php?city=okc&month=07&year=2003]

Riddle A., D. Carruthers, A. Sharpe, C. McHugh, and J. Stocker, 2004: Comparisons between FLUENT and ADMS for atmospheric dispersion modeling. *Atmos. Environ.*, **38**, 1029-1038.

Rotach, M.W., S.-E. Gryning, E. Batchvarova, A. Christen, and R. Vogt, 2004: Pollutant dispersion close to an urban surface – the BUBBLE tracer experiment. *Meteor. & Atmos. Phys.*, **87**, 39-56.

Rotach, M.W., 1999: On the influence of the urban roughness sublayer on turbulence and dispersion. *Atmos. Environ.*, **33**, 4001-4008.

Sagrado, A.P.G., J. van Beeck, P. Rambaud, and D. Olivari, 2002: Numerical and experimental modeling of pollutant dispersion in a street canyon. *J. Wind Eng. & Ind. Aerodyn.,* **90**, 321-339.

Scaperdas, A., and R.N. Colvile, 1999: Assessing the representativeness of monitoring data from an urban intersection site in central London, UK. *Atmos. Environ.*, **33**, 661-674.

Van Ulden, A.P., 1978: Simple estimates for vertical diffusion from sources near the ground. *Atmos. Environ.*, **12**, 2125-2129.

Venkatram, A., V. Isakov, D. Pankratz, J. Heumann, and J. Yuan, 2004: The analysis of data from an urban dispersion experiment. *Atmos. Environ.*, **38**, 3647-3659.

Wilson, D.J., and B.K. Lamb, 1994: Dispersion of exhaust gases from roof-level stacks and vents on a laboratory building. *Atmos. Environ.*, **28**, 3099-3111.
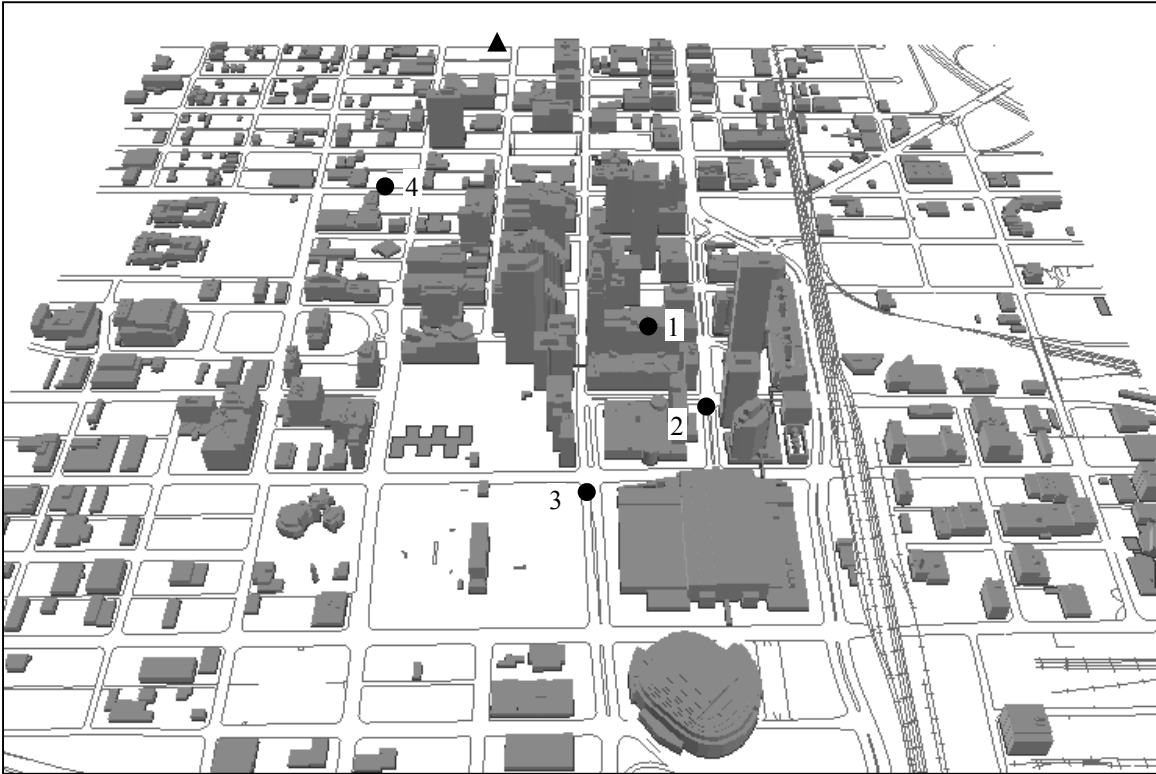
Figure 2-1. Downtown Oklahoma City urban landscape.
The measurement crane is marked with a triangle, and the release positions are marked with circles.

Sonic	Height AGL (m)	Tracer Inlet	Height AGL (m)
1	7.8	1	10.7
2	14.6	2	17.5
3	21.5	3	24.4
4	28.3	4	34.7
5	42.5	5	48.4
6	55.8	6	62.1
7	69.7	7	75.8
8	83.2		

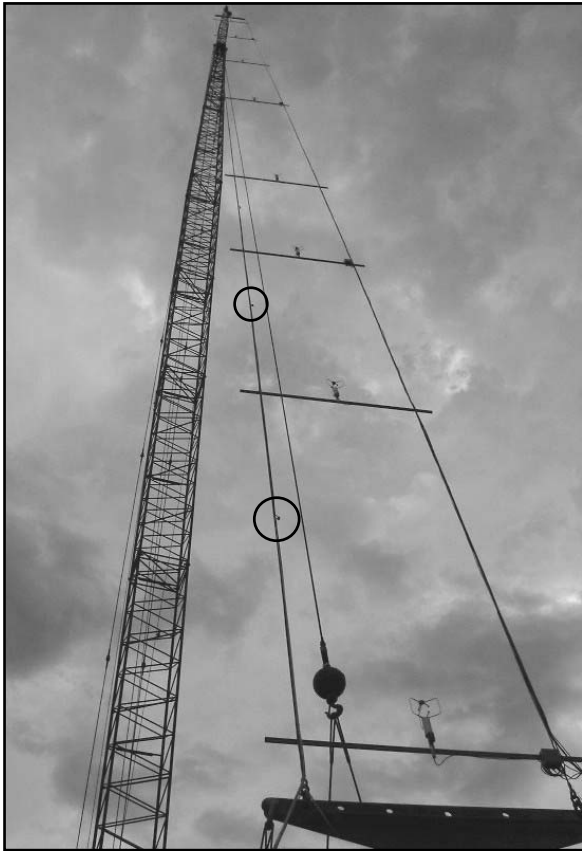Table 2-1. Sonic anemometer and tracer sample inlet heights at the crane site.

Figure 2-2. Instrumented crane system.
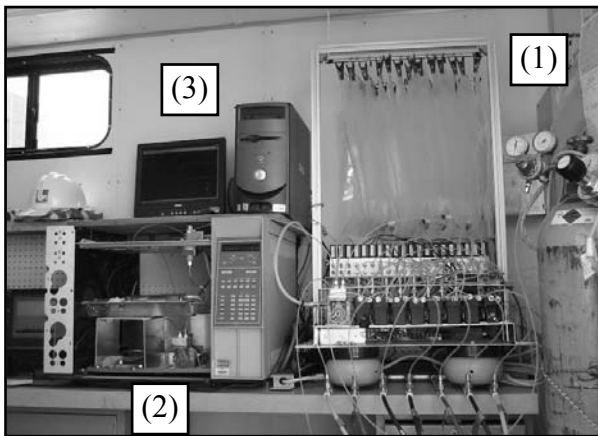Circles enclose the first two of the seven tracer inlets.

Figure 2-3. WSU Travert profile system: (1) sampling bags and valves, (2) SF_6 analyzer, and (3) control and data acquisition computer.

IOP	1	2	3	4	5	6	7	8	9	10
LDL (ppt)	21	26	25	19	12	8	10	8	9	10

Table 2-2. Lower SF_6 detection limits during each IOP.

IOP	1	2	3	4	5	6	7	8	9	10
CV	3.7%	6.2%	3.3%	1.1%	6.1%	5.8%	6.9%	4.2%	4.0%	4.5%
Gas	5.0%	5.0%	5.0%	5.0%	5.0%	5.0%	5.0%	5.0%	5.0%	5.0%
Total Error	6.2%	8.0%	6.0%	5.1%	7.9%	7.7%	8.5%	6.5%	6.4%	6.7%

Table 2-3. Estimated SF_6 calibration errors during each IOP.
CV = coefficient of variability of the span.

IOP	Date	DOY	Start (CDT)	End (CDT)	Release Location	WD (deg)	WS (m s^{-1})	Distance (m)
1	6/29/03	180	0900	1400	Modified 2	158	3.6	1005
2	7/2/03	183	0900	1600	2	205	4.4	995
3	7/7/03	188	0900	1600	3	190	5.8	1085
4	7/9/03	190	0900	1600	3	197	6.3	1085
5	7/13/03	194	0900	1630	3	173	3.9	1085
Mini	7/15/03	196	1200	1400	4	191	5.6	470
6	7/16/03	197	0900	1630	3	186	4.3	1085
7	7/18/03	199	2300	0630	3	213	4.1	1085
8	7/24/03	205	2300	0630	2	158	3.9	995
9	7/26/03	207	2300	0630	1	173	4.0	830
10	7/28/03	209	2100	0400	1	198	4.3	830

Table 2-4. Intensive operating period (IOP) summary.
Release locations are marked in Figure 1. Wind speed (WS) and wind direction (WD) values are from the z = 42.5 m level at the crane site. The distance is the straight-line distance between the source and crane locations.
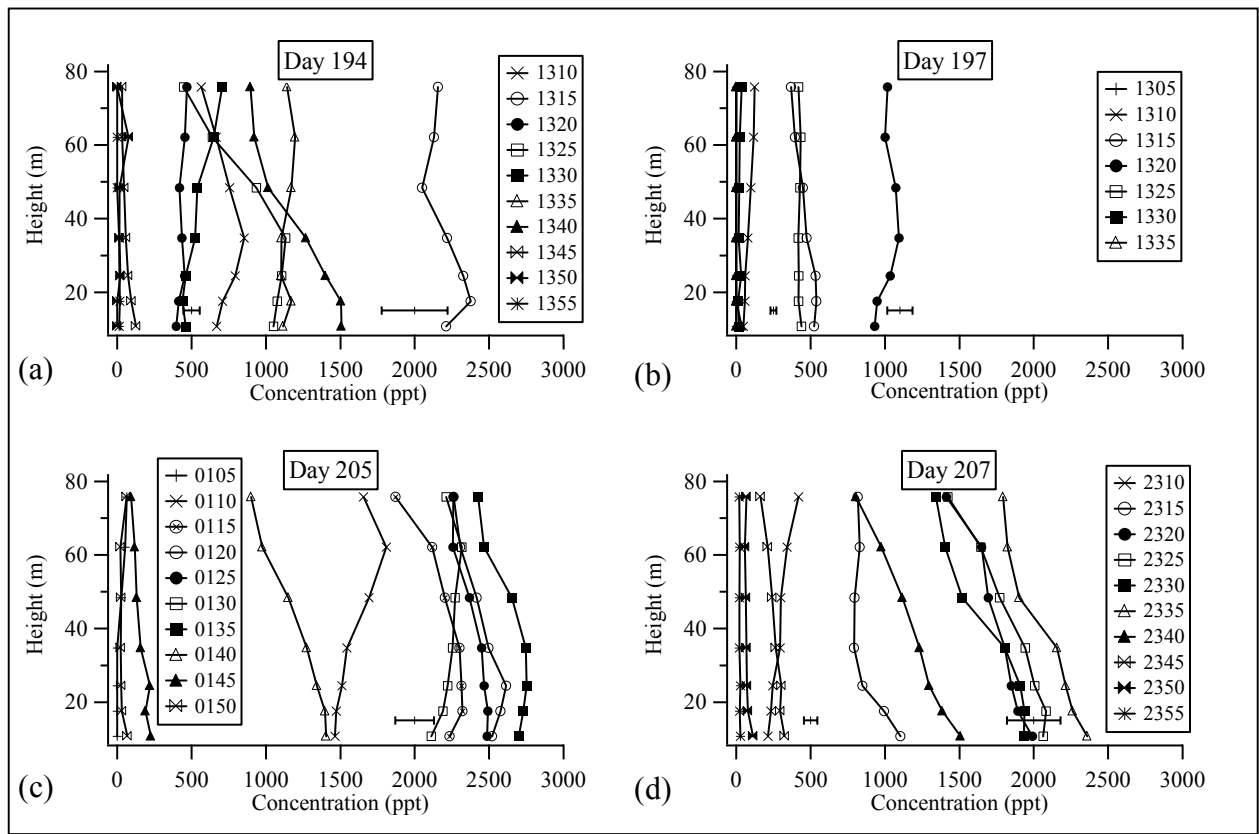
Figure 2-4. Concentration profiles from day (a) 194, (b) 197, (c) 205, and (d) 207.
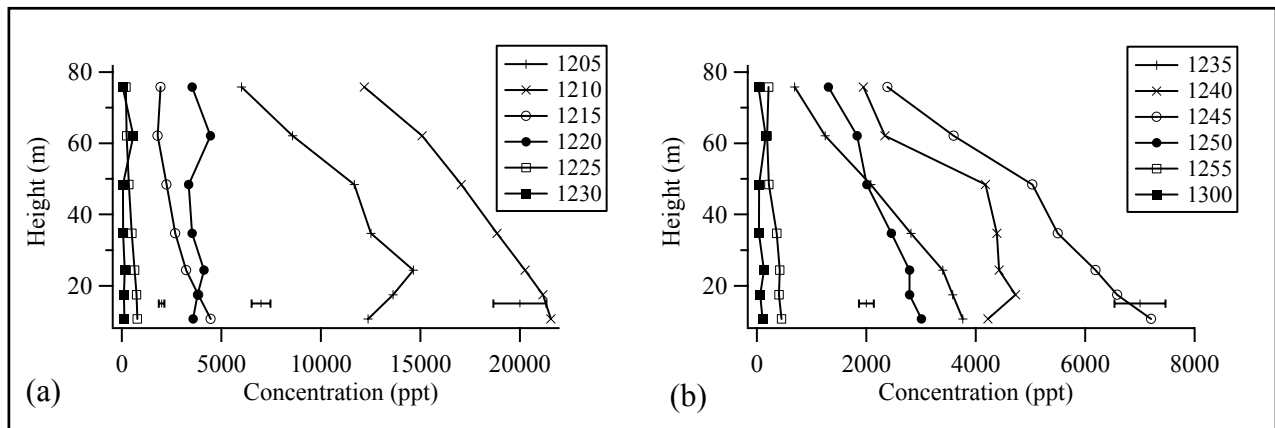The release rate was 3 g s^{-1} for (a) – (c) and 2 g s^{-1} for (d).

Figure 2-5. Concentration profiles from the Mini IOP.
Release rate was 8 g s^{-1} during (a) and 5 g s^{-1} during (b).
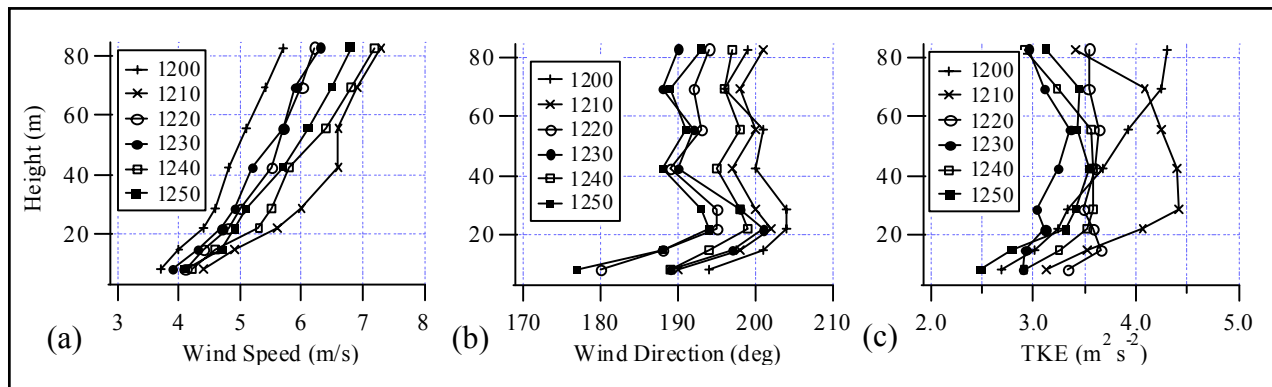

Figure 2-6. Vertical profiles of (a) wind speed, (b) wind direction, and (c) turbulent kinetic
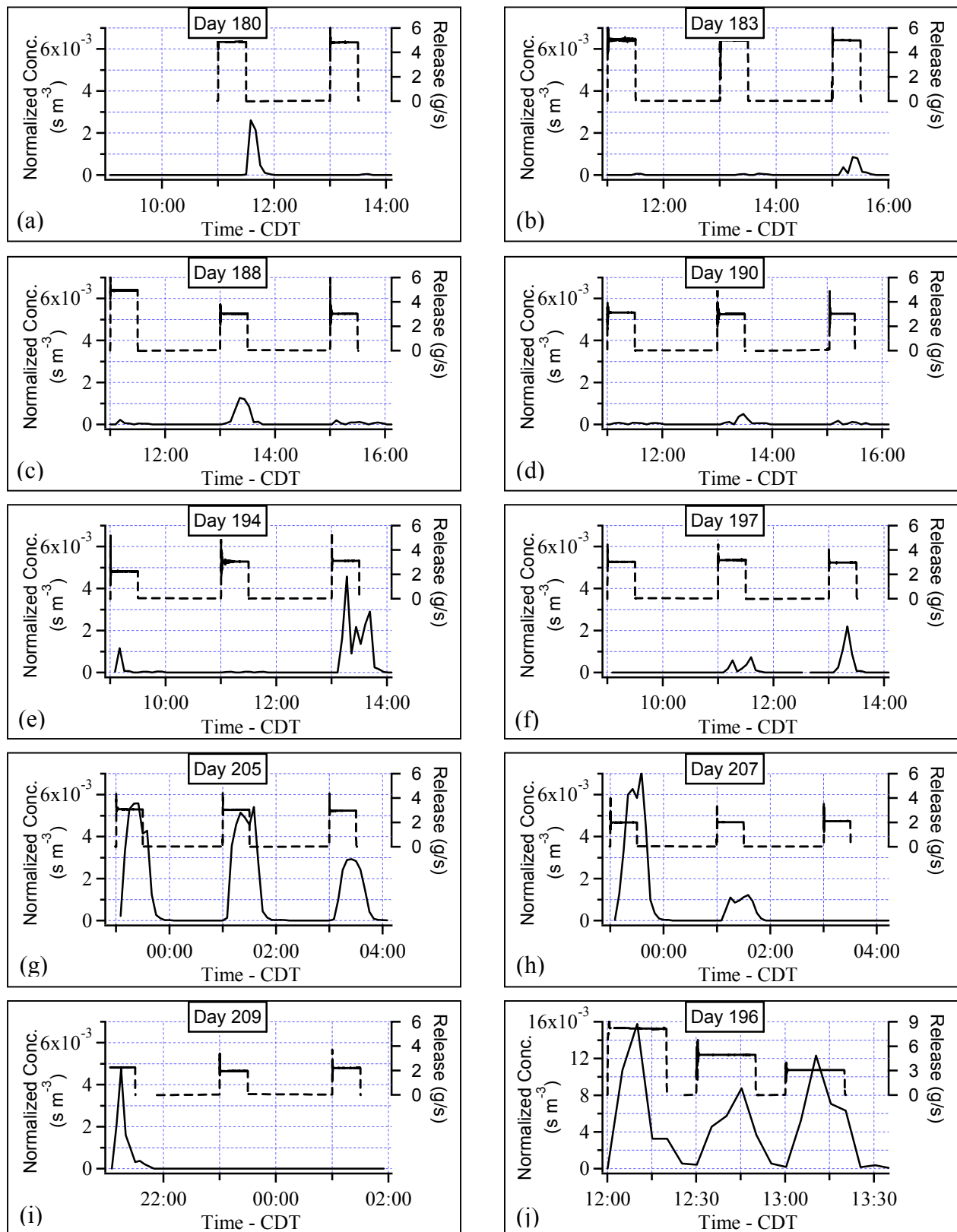energy from the Mini IOP.

Figure 2-7. Normalized SF$_6$ concentrations.
The y-axis range for Figure (j) is larger than the other figures because this was the Mini IOP, which had a much closer release point.
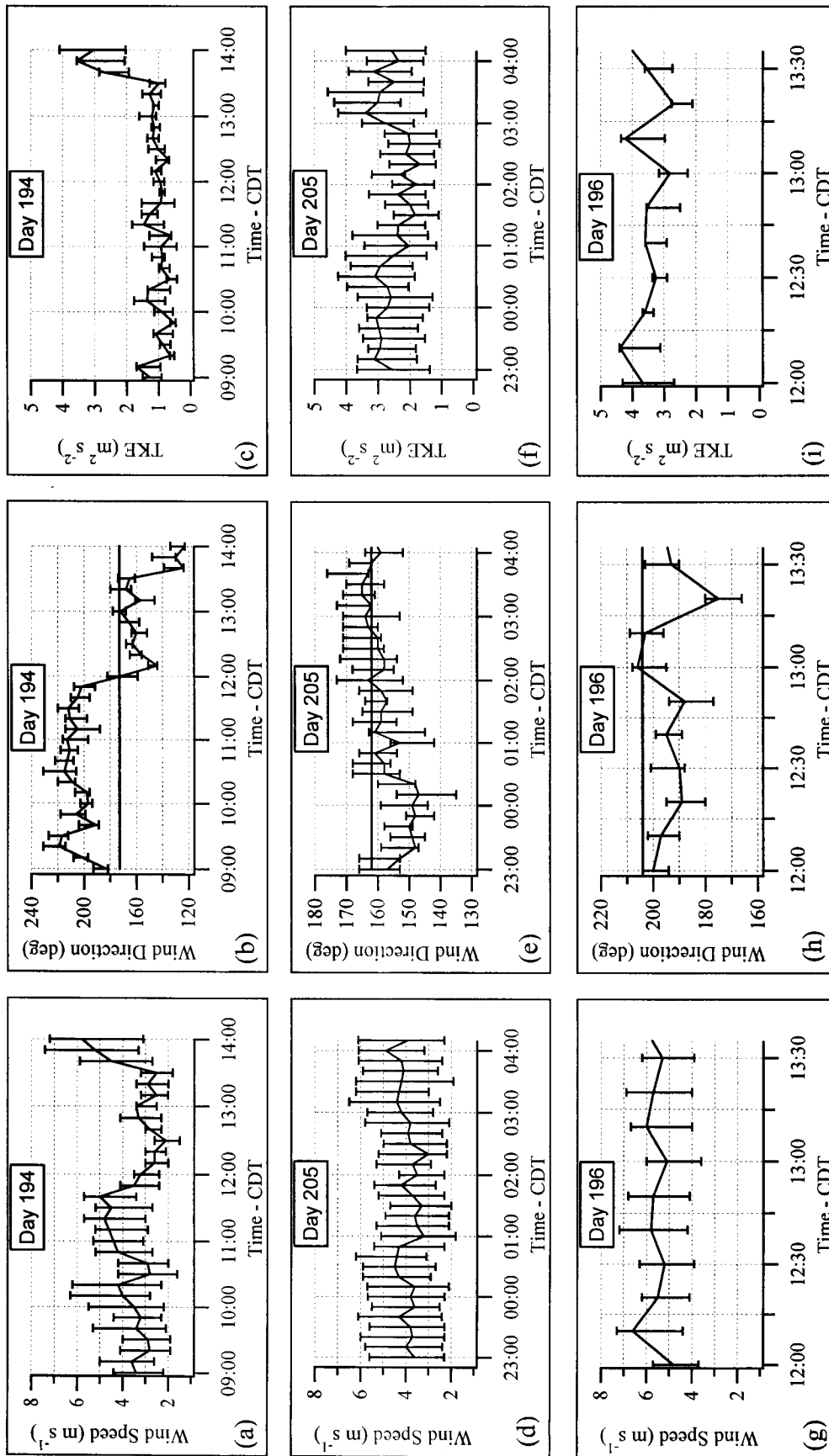
Figure 2-8. Wind speed, wind direction, and turbulent kinetic energy from the 42.5-m sonic on days 194 (a - c), 205 (d - f), and 196 (g - i). Error bars denote the range of values observed over the 8 levels that were monitored. The solid horizontal line on the wind direction plots denotes the azimuth connecting the release to the receptor.

35
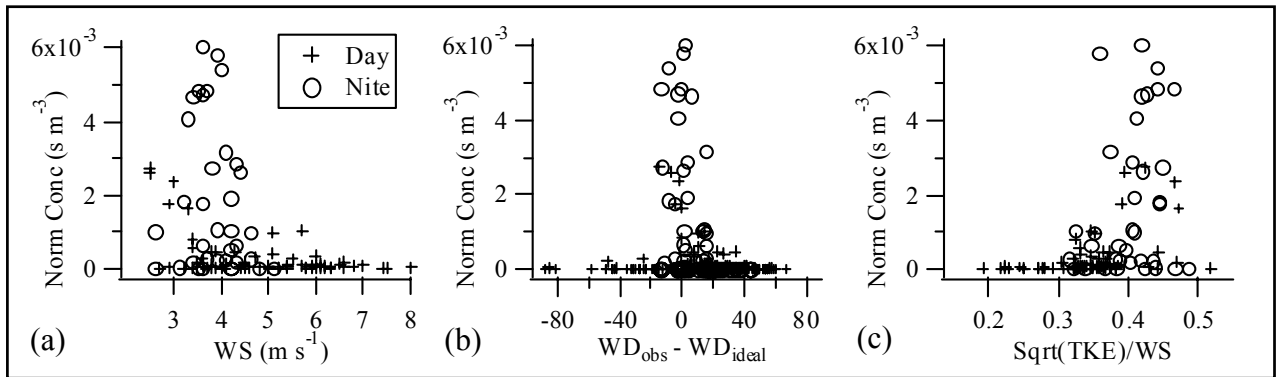
Figure 2-9. Scatter plots of normalized concentration versus (a) wind speed, (b) wind direction deviation from the ideal, and (c) turbulent intensity analog computed as the ratio of the square root of turbulent kinetic energy to wind speed.
Concentration values are the maximum over the depth of the profile, while meteorology values are from the 42.5-meter level.
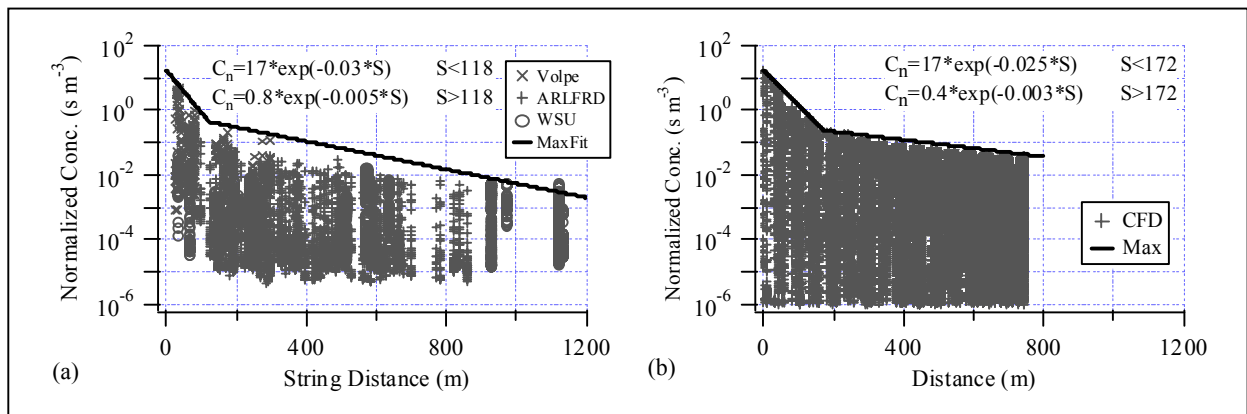
Figure 2-10. Maximum concentration curves from (a) 5-min bag samplers during 30-min continuous releases and (b) CFD analysis.
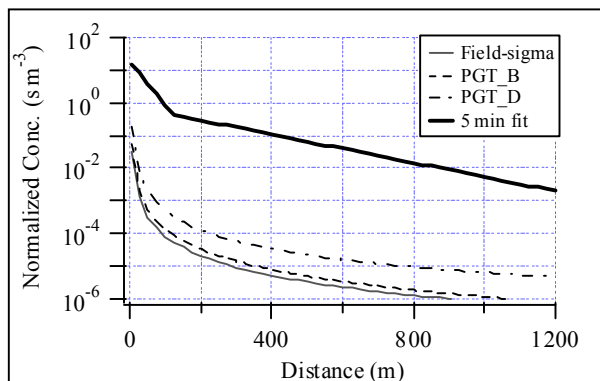
Figure 2-11. Comparison between maximum concentration from the Gaussian plume equation and fit from field data.

CHAPTER THREE

USING COMPUTATIONAL FLUID DYNAMICS TO MODEL URBAN DISPERSION

Julia Flaherty and Brian Lamb

Laboratory for Atmospheric Research, Department of Civil and Environmental Engineering,

Washington State University, Pullman, WA

David Stock

Department of Mechanical and Materials Engineering,

Washington State University, Pullman, WA

ABSTRACT

A 3D computational fluid dynamics study using the k-ε turbulence model was conducted and validated with field data from an urban dispersion study. The modeled flow field indicated that the many short buildings in this domain had a relatively small effect on the flow field, while the few tall buildings drove the transport and dispersion of tracer gas through the domain. Modeled concentrations and wind speeds were compared to observations along a vertical profile located about 500 meters downwind of the source. The isothermal base case was within 50% of the field measurements, while a convective case with ground and building surfaces 10 degrees C hotter than the air improved the modeled profile to within 30% of observations. Varying wind direction and source location had a significant effect on the plume dispersion due to the irregularity of the urban landscape. The location of the tallest obstacle in this domain with respect to the source position defined the size and shape of tracer plumes in this study.

1. Introduction

Urban air quality modeling and measurements pose many interesting challenges for atmospheric scientists and environmental engineers. For example, the urban environment is characterized by particularly complex flow patterns. These include separation, recirculation, channeling, and chimney effects. As such, pollutant plumes in the urban landscape can often travel non-intuitive paths. Britter and Hanna (2003) summarized the important features in urban areas and highlight research on moisture, heat, and roughness, as well as other parameters that affect urban flow patterns.

Urban environments are especially important in air quality studies because there is both a high occurrence of pollutant sources (such as vehicles) and receptors (people). According to a United Nations (2004) report, 48% of the world's population lived in urban areas in 2003. In order to protect these people from urban air pollutants, regulatory agencies require monitoring stations to ensure cities do not exceed pollutant standards. However, improperly sited monitoring stations may report less-than-typical concentrations, allowing urban populations to unknowingly experience unhealthy levels of pollutant. Alternately, monitors may report higher-than-typical concentrations, which causes cities to invest unnecessary funds into attainment plans.

As computing power has become more affordable, computational fluid dynamics (CFD) has become an increasingly valuable tool to study urban flow. These models explicitly account for building geometry, and require minimal parameterizations as compared to a Gaussian model. Knowledge gained from computational efforts can be used for guidance in urban design to explore pollutant "hot spots," minimizing personal exposure and ensuring proper positioning of air intakes for building HVAC systems.

In recent years, researchers have conducted CFD studies on various geometries. For example, there have been numerous investigations with single buildings, such as the work of Brzoska et al. (1997), Gao and Chow (2005), Meroney et al. (1999), Cowan et al. (1997), and Calhoun et al. (2004), ranging from a simple cube to a complex building. There has also been a great deal of study involving single street canyons. This work lends itself easily to two-dimensional investigation, such as the work of Jeong and Andrews (2002), Kim and Baik (2001), and Chan et al. (2002). Additionally, other groups, such as Lien and Yee (2004) and Chang and Meroney (2003) have examined generic arrays of building obstacles, while small groups of

buildings have been modeled by Guenther et al. (1990), Riddle et al. (2004), and Scaperdas and Colville (1999).

The objective of this paper is to present flow field and tracer dispersion results from a 3D CFD simulation based on data collected from the Joint Urban 2003 field campaign conducted in Oklahoma City. Section 2 briefly describes the field measurements used for this comparison. Section 3 presents the model set-up, while section 4 gives their results. Finally, conclusions and future work are presented in section 5.

2. Field measurements

The Washington State University (WSU) Laboratory for Atmospheric Research (LAR) participated in the Joint Urban 2003 field campaign by measuring tracer concentrations approximately 1 km from the tracer release. Continuous five-minute averaged concentrations of SF_6 tracer gas were measured at seven heights, from 10 to 75 meters above ground level. Eight sonic anemometers also collected data at this site continuously throughout the month-long study. Researchers from Lawrence Livermore National Laboratory (LLNL) collected the sonic anemometer measurements and processed 10-minute averaged values. The present study investigates a tracer release period that is referred to as the Mini intensive operating period (IOP). This case was selected primarily because the tracer release position was approximately 5 blocks, or 500 meters, upwind of the WSU/LLNL crane compared to the nearly 1 km distance between the source and receptor during other IOPs.

3. Numerical modeling

a. Computational domain

   The computational domain utilized for this study was 900 meters wide, 1200 meters

deep, and 300 meters tall. It incorporated about 40 city blocks: 5 east-west and 9 north-south.

The buildings within this domain were created using GAMBIT 2.2.30, a preprocessing program

for modeling geometry and creating mesh. Approximately 150 buildings with 1-meter resolution

were incorporated in this domain, which was located north of the central business district of

Oklahoma City, Figure 3-1. The buildings were irregularly spaced, and many of the buildings

had fairly small footprints. The tallest building was the 70-meter Regency Tower, which was

located near the center of the domain. There was a cluster of buildings that are about 50 meters

tall in the southeast corner of the domain, but most of the buildings were less than 10 meters tall.

The black circle in Figure 3-1 represents the location of the tracer release, while the triangle

represents the crane location.

   The domain was meshed with 3-m tetrahedral cells near the ground and faces of the

buildings. These cells were allowed to grow at a rate of 1.05 away from these surfaces to

minimize the computational effort associated with excess cells. Although hexahedral cells are

preferred for computational accuracy and efficiency, the geometry of the domain made it

particularly difficult to utilize hexahedral meshing. This meshing scheme created approximately

2,995,000 cells in the domain.

b. Model details

   In order to gain some insight into the mechanisms by which dispersion occurs in an urban

environment, a computational fluid dynamics analysis with a Reynolds Averaged Navier-Stokes

(RANS) model was conducted. Although the instantaneous Navier-Stokes equations exactly

define all fluid flow, it is essentially impossible to solve these equations for turbulent flows over

domains of significant spatial scale. Therefore, the exact equations are often Reynolds-averaged

to create a set of equations that can be solved for the spatial scales that we are interested in.

FLUENT 6.2.16 was employed in this modeling study. A steady-state computation with the

standard k-ε turbulence closure model was utilized. The k-ε models are known to have

weaknesses in complex flows, and incorrectly assume the dispersion coefficients are isotropic.

However, it is an appropriate model to begin this computation, as it requires less computational

effort compared to the Reynolds stress model (RSM) or large eddy simulation (LES).

The Reynolds-averaged Navier-Stokes (RANS) equations are

$$\frac{\partial \rho}{\partial t} + \frac{\partial}{\partial x_i}(\rho u_i) = 0 \text{, and} \tag{1a}$$

$$\frac{\partial}{\partial t}(\rho u_i) + \rho \frac{\partial}{\partial x_j}(u_i u_j) = -\frac{\partial p}{\partial x_i} - \rho g_i - \rho \beta (T - T_0) g_i + \frac{\partial^2 u_i}{\partial x_j^2} + \frac{\partial}{\partial x_j}(-\rho \overline{u_i' u_j'}), \tag{1b}$$

where (1a) is the continuity equation and (1b) is the momentum equation. The variables in these

equations are: ρ is the density, u_i, and u_j, are the velocity component in the x_i, and x_j, directions,

respectively, g is gravity, β is the thermal expansion coefficient, and T and T_0 are the

temperature and reference temperature. Here, the overbar (¯)and prime (´) denote the mean

and fluctuating components of the velocity.

The Reynolds stresses, the final term in equation (1b), must be modeled to develop a closed

set of equations. For the k-ε model, the Boussinesq hypothesis is utilized and the Reynolds

stresses are modeled in terms of the mean velocity gradients:

$$-\rho \overline{u_i' u_j'} = \mu_\tau \left(\frac{\partial u_i}{\partial x_j} + \frac{\partial u_j}{\partial x_i} \right) - \frac{2}{3} \left(\rho k + \mu_\tau \frac{\partial u_i}{\partial x_i} \right) \delta_{ij}. \tag{2}$$

μ_τ is the turbulent viscosity, k is the turbulent kinetic energy, and δ_{ij} is the kronecker delta. The turbulent kinetic energy (k) and turbulent dissipation rates (ε) were obtained from the following transport equations:

$$\frac{\partial}{\partial t}(\rho k) + \frac{\partial}{\partial x_i}(\rho k u_i) = \frac{\partial}{\partial x_j}\left[\left(\mu + \frac{\mu_T}{\sigma_k}\right)\frac{\partial k}{\partial x_j}\right] + G_k + G_b - \rho\varepsilon - Y_M + S_k, \text{ and} \tag{3}$$

$$\frac{\partial}{\partial t}(\rho\varepsilon) + \frac{\partial}{\partial x_i}(\rho\varepsilon u_i) = \frac{\partial}{\partial x_j}\left[\left(\mu + \frac{\mu_T}{\sigma_\varepsilon}\right)\frac{\partial\varepsilon}{\partial x_j}\right] + C_{1\varepsilon}\frac{\varepsilon}{k}(G_k + C_{3\varepsilon}G_b) - C_{2\varepsilon}\rho\frac{\varepsilon^2}{k} + S_\varepsilon. \tag{4}$$

G_k and G_b are the generation of turbulence kinetic energy due to the mean velocity gradients and to buoyancy, respectively. Y_M is known as the dilatation dissipation, which is neglected for incompressible flows. $C_{1\varepsilon}$, $C_{2\varepsilon}$, and $C_{3\varepsilon}$ are constants, σ_k and σ_ε are the turbulent Prandtl numbers for k and ε, and S_k and S_ε are user-defined source terms. (Fluent, Inc., 2003)

The turbulent viscosity was modeled as

$$\mu_t = \rho C_\mu \frac{k^2}{\varepsilon}. \tag{5}$$

The constants in standard k-ε model were from Launder and Spaulding (1972):

$$C_\mu = 0.09 \qquad \sigma_k = 1 \qquad \sigma_\varepsilon = 1.3 \qquad C_{\varepsilon 1} = 1.44 \qquad C_{\varepsilon 2} = 1.92$$

The SIMPLE pressure-velocity coupling algorithm was utilized to enforce mass conservation. To minimize numerical diffusion, the second order upwind discretization scheme was utilized for this computation. Gradients were computed using the node-based option, which is known to be more accurate than a cell-based scheme for tetrahedral cells. Finally, standard wall functions were used to account for the effect of the walls.

c. Boundary conditions

We simulated a continuous release of SF_6 tracer that was conducted at 1240 CDT on July 15, 2003. The 10-minute average wind direction during this study was 197 degrees, and the sides of the domain were parallel to the mean wind direction. This allowed these sides to be prescribed as symmetry conditions, and the south and north boundaries were velocity inlet and outflow conditions, respectively. The ground and walls of the buildings were defined as stationary walls with appropriate roughness applied. Aerodynamic roughness lengths (z_o) of 0.1 and 0.05 m for the ground and building surfaces were approximated from Stull (1988). The corresponding roughness height was computed as 1.95 m and 0.98 m. Lastly, the ceiling was set as a moving wall.

The velocity inlets were defined with wind speed, turbulent kinetic energy, and turbulent dissipation rate profiles. An initial wind speed profile was defined by fitting a logarithmic profile to the 10-minute averaged data from the eight sonic anemometers that were mounted on the crane. This profile compared well with sodar data from three different sites that were both upwind and downwind of the crane. This gives us confidence that the profile chosen was representative of the mean flow over the city. Turbulent kinetic energy and turbulent dissipation rate profiles were adapted from Detering and Etling (1985). These initial inlet profiles were adjusted to physically match each other by running it through a generic section of the Oklahoma City urban landscape. See Figure 3-2 for the inlet profiles used for these computations.

d. Model cases

In order to fully characterize urban dispersion in this landscape, several model cases were investigated. The base case was an isothermal investigation of the 197-degree wind direction.

The flow field was computed for a total of 600 iterations on four nodes of a Linux cluster. The computation required approximately 45 seconds per iteration for a total of 7.5 hours. The tracer concentrations were computed using the turbulent Schmidt number of 0.7 to relate diffusivity of momentum to the diffusivity of a tracer species. SF_6 was released from a 4.4-m^3 volume about 2 meters above the ground at a rate of 5 g s^{-1}. Ten iterations were performed with the species model to ensure that the residuals were low.

The Regency Tower was a significant obstacle between the source location and the crane site. Therefore, we also considered a case in which this large building did not exist. This showed the effect that this particular obstacle had on flow and dispersion and illustrated the importance of including all the buildings in the domain. In modeling urban environments, there is often a challenge associated with verifying the accuracy of the urban landscape. Databases can often be outdated, but including the correct building dimensions is far less important than simply knowing that a building exists at a specific location.

To explore both the sensitivity of the tracer concentration at the crane site to wind direction and the potential effect of wind direction variability over this 10-minute period, two additional wind direction cases were considered. Field measurements indicated that the standard deviation of the wind direction was approximately 15 degrees. Therefore, 182-degree and 212-degree wind direction cases were computed.

In addition to variability in wind direction, the effects of perturbing the source location were investigated. For these cases, the release was moved 50 meters to the east and the west and 15 meters vertically from the base case location. A final source location case moved the source just 2 meters downwind from the base case. This was conducted to see if there is any advantage, at this mesh resolution, to moving the source to a position in which the size of the cell (or

multiple cells, in this case) nearly matches the size of the plume. The plume width was determined by utilizing both the guidance of the Pasquill-Gifford Turner dispersion curves for urban landscapes and the variability in wind speeds from the field data.

Finally, the particular field case that we modeled was conducted at 1240 daylight time on a fairly hot summer day. Since the building surface temperature was greater than that of the surrounding air temperature, a case with thermal buoyancy was considered. A slightly unstable temperature profile was prescribed for the inlet air, and the ground and building surfaces were assumed to be 10 degrees hotter than the ground-level air temperature. Berdahl and Bretz (1997) show surface temperatures can exceed air temperatures by between 5 and 50 degrees C, depending on the color and type of material. Since this was a simple case to observe the effect of convection, 10 degrees was selected as something of an average temperature for the ground and building surfaces. In reality, the building rooftops would have the highest surface temperature, the building walls would have varying temperatures depending on the sun angle and shading, and the ground would also have spatially variable temperatures that depend both on shading and surface types. The Boussinesq approximation, which assumes the density is a function of temperature in the buoyancy term of the momentum equation, and constant for all other terms, was utilized for this model case.

In summary, the following cases were conducted:

a. Base case

b. Regency Tower removed

c. Changes in wind direction

   o + / - 15 degrees

d. Changes in source location

- o + / - 50 meters east

- o + 15 meters vertically

- o + 2 meters north

e. Add heat

e. Grid uncertainty

Although the general patterns of flow parameters developed from this CFD analysis indicated that it produced physically realistic results, a more quantitative analysis of the computational error was necessary. Richardson extrapolation (Richardson, 1910), was used to determine the error associated with the computational grid. Celik and Karatekin (1997) provided a concise Richardson extrapolation procedure, which was utilized as a guide for this analysis. Three mesh sizes, nominally 3-, 4.2-, and 6-meter resolution tetrahedral cells, with 2,995,000, 1,415,000, and 664,000 cells respectively, were considered for this error analysis. The plume width at half maximum was selected as a parameter for the quantification of the grid error. This was selected because it is an integral quantity that exhibited monotonic convergence between the three mesh sizes. Since second order upwind discretization was used in the CFD modeling, a value of two was used to calculate estimates of the computational error. The grid convergence index, which is a conservative estimate of the error band (Celik and Karatekin, 1997), was 6% for the tracer plume half-max width. This shows that the errors associated with the base case grid size are relatively small, and that the mesh resolution utilized in this study is sufficient.

4. Results

a. Base case

First, we consider the flow field of the base case with the wind at 197 degrees. Figure 3-3 shows the velocity vectors on a plane 10 meters above ground level. The vectors cover many of the buildings, and the velocity above the shorter buildings do not appear to be perturbed significantly by the presence of these buildings. Vectors on the western half of the domain generally maintain a uniform direction. The taller buildings, however, alter velocity vectors in the eastern half of the domain, where the flow appears to travel towards the northeast corner.

If the velocity vectors are considered more closely, we clearly see how the smaller buildings have a much more subtle impact on the flow field compared to the overwhelming changes in flow direction observed near large buildings. Figure 3-4 presents the velocity vectors on a horizontal plane, three meters above the ground. Once again, the black dot represents the position of the tracer release. With the exception of the Regency Tower, located in the upper portion of the figure and marked with an "X," all of these buildings are rather small and short. The flows around these small buildings tend to wrap gently around the obstructions, and quickly return to the mean wind direction behind the buildings. There are no visible recirculation zones near the source.

Figure 3-5, on the other hand, shows a dramatic modification in the flow field caused by the obstruction of the Regency Tower. Vectors in this figure are again on the three-meter plane above the ground, and an "X" marks the Regency Tower. Flow approaching the building is nominally parallel to the mean wind direction, and separates around the building to create two counter-rotating vortices in the lee of this building. These flow features as well as the channeling seen between the buildings northeast of the Regency Tower play a significant role in determining the size and shape of the pollutant plume.

To develop a more three-dimensional view of the flow pattern over the Regency Tower, velocity vectors on a vertical plane are presented in Figure 3-6. This vector plot depicts flow features that are expected over such a building. There is a relatively small recirculation zone near the ground upwind of the building, which corresponds to velocity vectors moving down the upwind face. Conversely, the larger vortex downwind of the building corresponds to winds flowing up the downwind face. This figure indicates how tall buildings can very effectively mix the tracer plume.

Figure 3-7 presents concentration contours from 0.1 to 1 x 10^6 parts per trillion by volume (ppt). This figure reflects the flow field observed in previous graphs, with the plume centerline appearing to follow the upper-level wind direction initially, then displaying some asymmetry due to the mixing by the taller buildings toward the east of the plume centerline. The contours are very close to each other on the western half of the plume, while there are large spaces between contour lines on the eastern half. This shape is created initially by the Regency Tower, and is exacerbated by the channeling and mixing from the tall buildings to the northeast of the tower.

Vertical profiles of velocity, turbulent kinetic energy (TKE), turbulent dissipation, and tracer concentration from the model at the WSU/LLNL crane site are presented in Figure 3-8. The range on the vertical axis in both the dissipation rate and concentration plots goes only to 100 meters in order to show more detail. The profiles of velocity, TKE, and turbulent dissipation rate have general shapes that we expect in an urban environment. Buildings upwind of this site depress the velocities at low elevations, but comparing with the field data suggests that the model has overestimated the effect of the buildings. Near the ground, the model predicts about half of the observed wind speed. The turbulent kinetic energy peaks at about 50 meters height with a

value of about 1.5 m^2 s^{-2}. Although the shape of the TKE profile compares well with the field

data, the magnitude of the profile is underestimated. The field data TKE peaks at a value of

about 3.6 m^2 s^{-2}. The upwind buildings, and in particular, the Regency Tower, likely defines

both the magnitude and height of the TKE peak. The turbulent dissipation rate profile also has a

local maximum at around 50 meters. Generally, the dissipation rate decreases with increasing

height. The modeled tracer concentration profile compares fairly well with observations.

Modeled values are generally within 50% of the observations, with overestimation below about

50m, and underestimation above 50m.

b. Regency Tower removed

For comparison, the contours of SF_6 concentration on the z=10m plane for the domain

without the Regency Tower are presented in Figure 3-9. As expected, the plume is much more

symmetrical about the centerline. The eastern half of the plume is still wider than the western

half, indicating that this feature is indeed a result of the channeling between and mixing by the

taller buildings in this part of the plume.

The profiles at the crane site for this case are also presented in Figure 3-8. The velocity

defect is not as severe for this case, and compares well with the upper half of the sonic

anemometer measurements. The shape of the TKE curve is similar to the base case; however,

the maximum value of about 1.2 m^2 s^{-2} occurs at about 30 meters, nearly half the height of the

base case. Correspondingly, the turbulent dissipation rate profile has smaller values at high

vertical positions than in the base case. There is less energy generated in this case, and therefore

less energy to dissipate as well. As one would expect, removing the Regency Tower has a

significant effect on the concentration observed at this downwind position. At the top receptor,

the concentration is very similar to the observations; however, with decreasing height, the concentration is increasingly overestimated. Near the ground, the concentrations are nearly 5 times the observation. This single, large obstacle mechanically mixes the plume in the vertical direction to decrease the gradient of the concentration profile.

c. Changes in wind direction

Figure 3-10 presents the concentration contour plots on the z=10m plane for the two additional wind direction cases. For the 182-degree case, the large and tall buildings were well to the right of the plume centerline, which allowed for a rather narrow plume overall. The crane location was near the edge of this plume, so very low concentrations were expected. When the wind direction was 212 degrees, however, the tallest buildings were very near the centerline of the plume, which resulted in a rather wide plume.

The vertical profiles at the crane position for the three different wind direction cases are compared in Figure 3-11. Interestingly, the velocity magnitude profiles for all three cases were very similar to each other. The crane was located in a clearing, with about 100 meters of empty space upwind. Therefore, it appears that velocity profile develops over the length of this clearing, so any southerly wind results in nominally the same profile. The turbulent kinetic energy profile, on the other hand, still reveals dependence on the upwind building characteristics. The 182-degree case has a TKE profile very similar to the 197-degree base case. The 212-degree case, on the other hand, was more similar to the "no Regency" case, a result of shorter buildings upwind of the receptor. The turbulent dissipation rate profiles were very similar between the three cases, with slight differences between 40 and 100 meters above the ground. Finally, the tracer concentration profile showed exactly what we expected from these three wind

51

direction cases. The base case results in the best comparison with field data, while concentrations were overpredicted and underpredicted by the 212-degree and 182-degree wind directions, respectively.

d. Changes in source location

Figure 3-12 presents the vertical concentration profiles for the four cases in which the source location was moved. When the source position was moved 50 meters to the east and west, along the length of the street, the effect on the concentration profile at the crane site was similar to the varying wind direction cases. Fifty meters is about one-third the length of the city block, so this indicates that it is very important to know the position of a point source as precisely as possible. When a hazardous spill or intentional release occurs, this may be one of the most difficult parameters to achieve, but can account for 2 orders of magnitude difference in concentration at a particular receptor.

Moving the source vertically by 15 meters, on the other hand, had a smaller effect on downwind concentrations. Concentrations were about double the base case near the ground, but approach the base case profile with increasing height. The higher concentrations were a result of fewer obstructions to the plume in the first few meters of transport. The original source height of about 2 meters was below the tops of the closest buildings, but the 17-meter height of the elevated source was well above these near-source buildings. The final source position was the 2-meter downwind shift that moved the source into two cells to match the approximate width of a Gaussian plume. Very little change is seen between the shapes of the concentration profiles for the base case and this Gaussian source shift case. Releasing the tracer from the downwind cells improved the agreement with the field data by about 10% at the lower receptors. This small

difference is likely because the original source cell was conveniently oriented. The tip of the tetrahedral source cell was at the true source location, while base of the cell was north of the tip. This shape mimics the spreading of the plume, so that moving the source to a wider downwind set of cells does little to improve the release volume.

e. Add heat

Figure 3-13 compares the velocity magnitude, turbulent kinetic energy, turbulent dissipation rate, and concentration profiles from the base case with the thermal buoyancy case in which surface temperatures were higher than the air temperature. Adding heat slightly improved the velocity magnitude predictions over the base case; however, wind speeds near the ground were still under-predicted. The turbulent kinetic energy profile, however, showed a significant improvement over the isothermal base case. The two cases were similar in that the peak TKE occurred at the same height, but TKE values were much higher when heat was added. Additionally, TKE values were larger than $1 \text{ m}^2 \text{ s}^{-2}$ for much of the upper half of the vertical profile when heat was added, whereas the TKE value was essentially zero above 150m in the base case. This case also shows better agreement with the field measurements of tracer concentration than the base case, with the change in the slope of the concentration profile attributable to thermal mixing lifting the plume. The lowest four receptors, which show the largest error, were 20% to 30% greater than the field data. Although only an approximate average surface temperature was applied, the qualitative improvement in the tracer profile comparison indicates that detailed building shading schemes may not be as important as simply prescribing the differential temperature between the surface and the air.

5. Conclusions and future work

This paper compared results of CFD modeling with the data collected during the Joint Urban 2003 atmospheric dispersion study. The flow field appeared quite reasonable and exhibited features that were expected in an urban environment. Furthermore, a grid uncertainty analysis conducted with this mesh revealed a grid uncertainty index of approximately 6%. Consequently, the mesh did not heavily influence the solution obtained from this analysis.

These results show that a single large obstacle can have a significant effect on the flow field, and that it is particularly important to model each building that exists between the source and receptor. The tracer concentration results showed that large obstacles significantly alter the plume shape. The plume in this study is asymmetric, with a pocket of highly mixed air behind the Regency Tower as well as channeling between buildings in the east half of the plume. The vertical concentration profile at the crane site was modeled with modest accuracy, with some error in the vertical gradient. This numerical investigation highlights an important difference between flows in urban cores and the slightly less developed areas that surround these cores. Downtown areas contain many tall buildings in a somewhat homogeneous array; however, dispersion in surrounding areas may be highly sensitive to a few key features in the landscape.

A survey of various modeling cases affirms that wind direction and source location are very important parameters for defining dispersion patterns. Flow traveling through irregular arrays of obstacles result in very different plumes depending on the localized landscape that it travels through. In this case, any plume whose centerline passed through the Regency Tower resulted in a very wide, relatively dilute plume, whereas centerlines that missed this obstacle produced much more narrow and concentrated plumes. This is particularly important to consider

when providing tools to emergency response personnel. In the event of a hazardous release, it is unlikely that the meteorology will be fully characterized, or that the source location will be known to high accuracy. Therefore, multiple modeling cases should be performed to provide several possible outcomes for consideration.

Future work with computational fluid dynamics modeling will include a number of improvements to the numerics. First, a more sophisticated approach to the convective case will be considered to determine the importance of applying more realistic temperatures to building and ground surfaces, including sun angle and building shading. Additionally, the isotropic dispersion defined by the k-ε model can be overcome by employing other turbulence closure models, such as the Reynolds stress model and large eddy simulation. These models allow anisotropy of turbulence and will likely produce a more accurate solution to the concentration field.

6. ACKNOWLEDGEMENTS

REFERENCES

Berdahl, P., and S.E. Bretz, 1997: Preliminary survey of the solar reflectance of cool roofing materials. *Energy and Buildings*, **25**, 149-158.

Britter, R.E., and S.R. Hanna, 2003: Flow and Dispersion in Urban Areas. *Annu. Rev. Fluid Mech.*, **35**, 469-496.

Brzoska, M.A., D. Stock, and B. Lamb, 1997: Determination of plume capture by the building wake. *J. Wind Eng. & Ind. Aerodyn.,* **67**, 909-922.

Calhoun, R., F. Gouveia, J. Shinn, S. Chan, D. Stevens, F. Lee, and J. Leone, 2004: Flow around a complex building: comparison between experiments and a Reynolds-averaged Navier-Stokes approach. *J. Appl. Meteor.*, **43**, 696-710.

Chan, T.L., G. Dong, C.W. Leung, C.S. Cheung, and W.T. Hung, 2002. Validation of a two-dimensional pollutant dispersion model in an isolated street canyon. *Atmos. Environ.*, **36**, 861-872.

Chang, C., and R.N. Meroney, 2003. Concentration and flow distributions in urban street canyons: wind tunnel and computational data. *J. Wind Eng. & Ind. Aerodyn.,* **91**, 1141-1154.

Celik, I., and O. Karatekin, 1997: Numerical experiments on application of Richardson extrapolation with nonuniform grids. *J. Fluids Eng.*, **119**, 584-590.

Cowan, I.R., I.P. Castro, and A.G. Robins, 1997: Numerical Considerations for Simulations of Flow and Dispersion Around Buildings. *J. Wind Eng. & Ind. Aerodyn.,* **67 & 68**, 535-545.

Detering, H.W., and D. Etling, 1985: Application of the E-ε turbulence model to the atmospheric boundary layer. *Boundary-Layer Meteor.*, **33**, 113-133.

Fluent Inc., 2003: Fluent 6.1 User's Guide. URL: http://www.fluentusers.com

Frietas, C.J., 1993: Journal of Fluids Engineering editorial policy statement on the control of numerical accuracy. *J. Fluids Engineering*, **115**, 339-340.

Gao, Y., and W.K. Chow, 2005. Numerical studies on air flow around a cube. *J. Wind Eng. & Ind. Aerodyn.*, **93**, 115-135.

Guenther, A., B. Lamb, and E. Allwine, 1990. Building Wake Dispersion at an Arctic Industrial Site: Field Tracer Observations and Plume Model Evaluations. *Atmos. Environ.*, **24A** (9), 2329-2347.

Jeong, S.J., and M.J. Andrews, 2002. Application of the k-ε turbulence model to the high Reynolds number skimming flow field of an urban street canyon. *Atmos. Environ.*, **36**, 1137-1145.

Kim, J., J. Baik, 2001. Urban street-canyon flows with bottom heating. *Atmos. Environ.*, **35**, 3395-3404

Launder, B.E., and D.B. Spalding, 1972. Lectures in mathematical models of turbulence. Academic Press, London, England.

Lien, F., and E. Yee, 2004: Numerical modeling of the turbulent flow developing within and over a 3-D building array, Part I: A high-resolution Reynolds-averaged Navier-Stokes approach. *Boundary-Layer Meteor.,* **112**, 427-466.

Meroney, R.N., B.M. Leitl, S. Rafailidis, and M. Schatzmann, 1999: Wind-Tunnel and Numerical Modeling of Flow and Dispersion about Several Building Shapes. *J. Wind Eng. & Ind. Aerodyn.,* **81**, 333-345.

Richardson, L.F., 1910: The approximate arithmetical solution by finite differences of physical problems involving differential equations, with an application to the stresses in a masonry dam. *Philos. Trans. Roy. Soc. London*, **A 210**, 307-357.

Riddle A., D. Carruthers, A. Sharpe, C. McHugh, and J. Stocker, 2004: Comparisons between FLUENT and ADMS for atmospheric dispersion modeling. *Atmos. Environ.*, **38**, 1029-1038.

Scaperdas, A., and R.N. Colvile, 1999: Assessing the Representativeness of Monitoring Data from an Urban Intersection Site in Central London, UK. *Atmos. Environ.*, **33**, 661-674.

Stull, R.B., 1988: *An Introduction to Boundary Layer Meteorology.* Kluwer Academic Publishers. 670 pp.

United Nations. 2004. World urbanization prospects: The 2003 revision. URL: http://www.un.org/esa/population/publications/wup2003/WUP2003Report.pdf
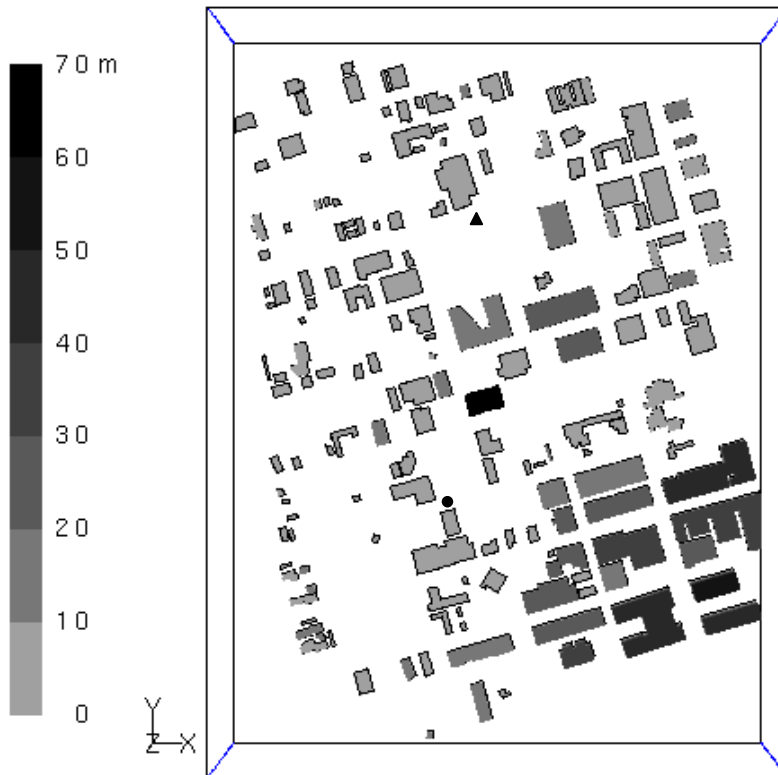
Figure 3-1. Computational domain.
    Buildings are shaded by height. The release and crane locations are marked with a
    black dot and triangle, respectively.

(a) Velocity Magnitude (m s^{-1})   (b) Turbulent Kinetic Energy (m^{2}s^{-2}) (c) Turbulent Dissipation Rate (m^{2}s^{-3})
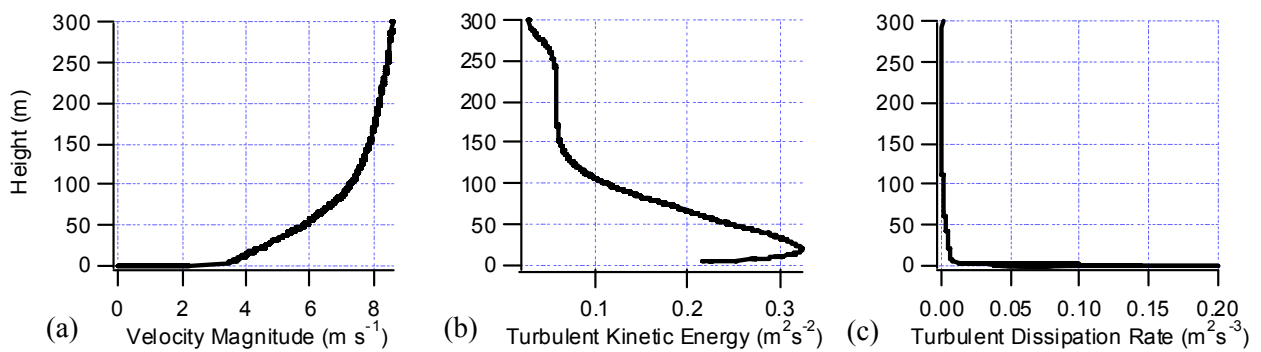
Figure 3-2. Velocity-inlet profiles.
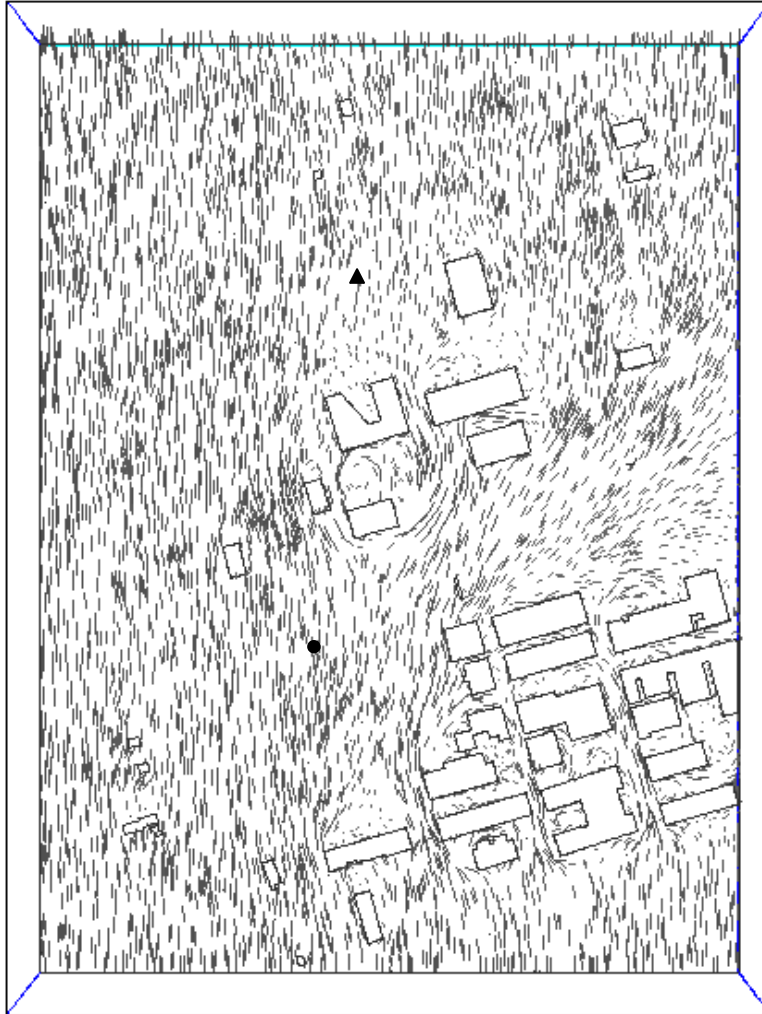
Figure 3-3. Velocity vectors on the z = 10-m plane.
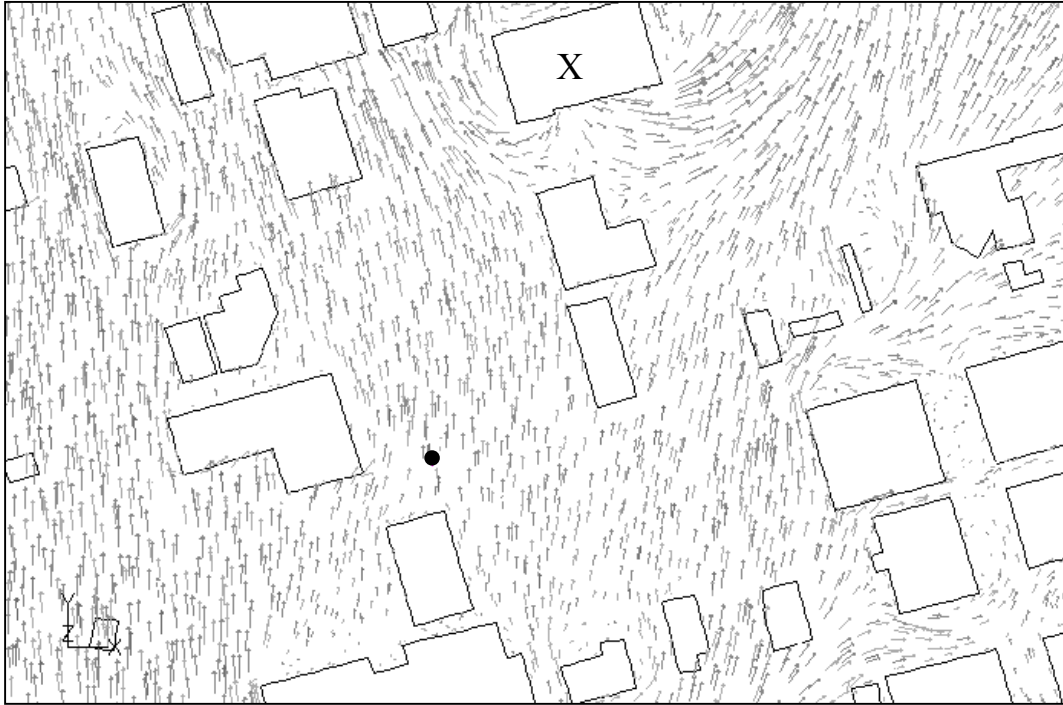
Figure 3-4. Velocity vectors near the release position on the z = 3-m plane.
The "X" marks the Regency Tower.
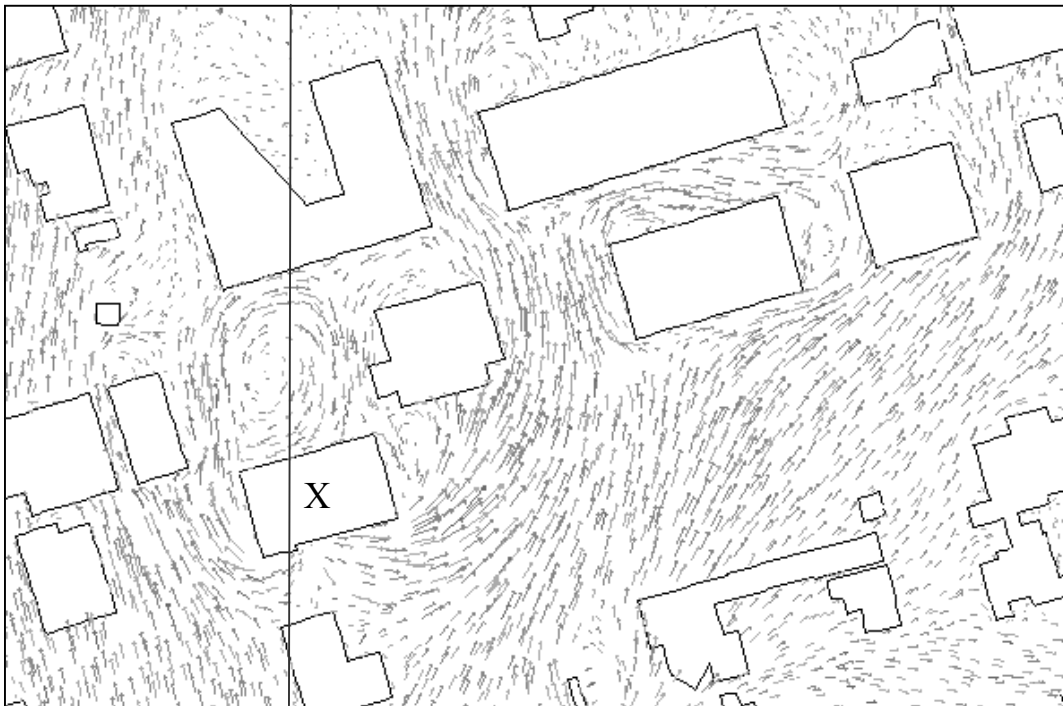
Figure 3-5. Velocity vectors near the Regency Tower on the z = 3-m plane.
The "X" marks the Regency Tower. The line going through the Regency Tower
represents the vertical plane shown in Figure 3-6.
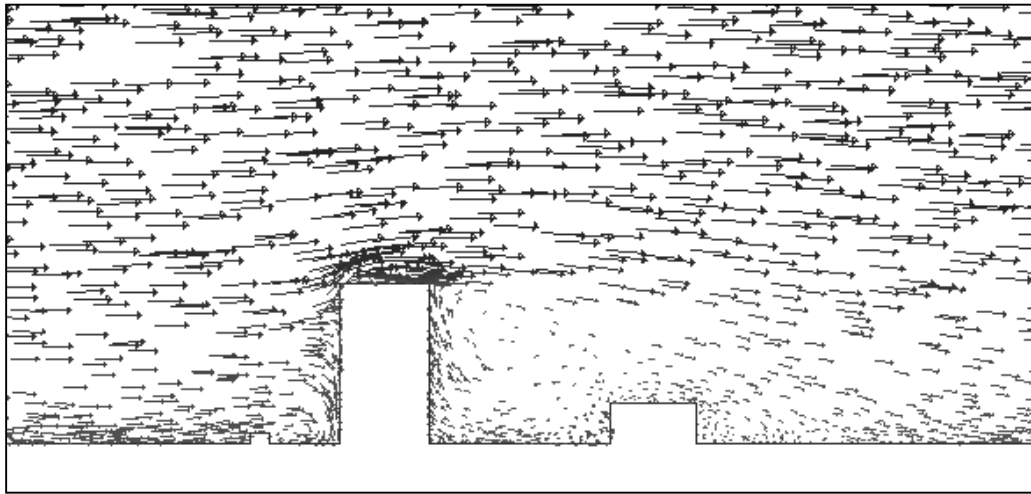
Figure 3-6. Velocity vectors over the Regency Tower on a vertical plane parallel to the sides of the domain.
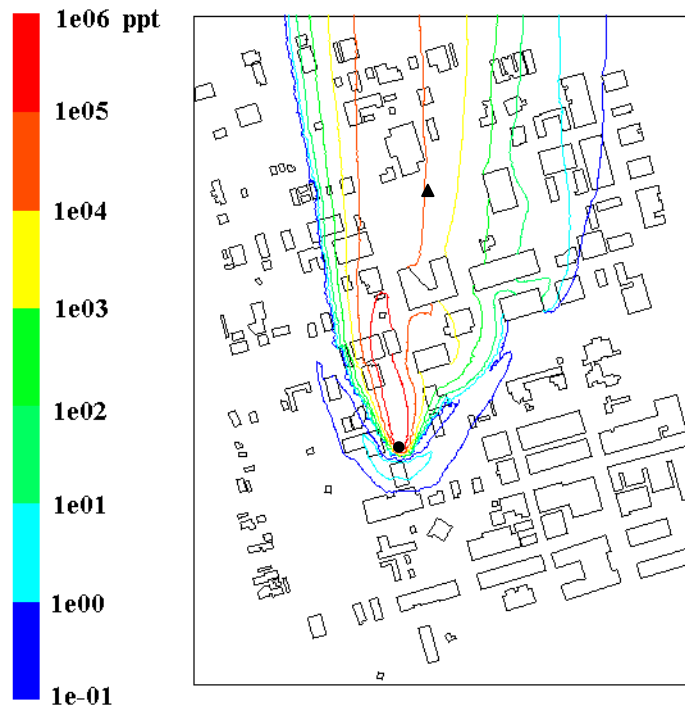
Figure 3-7. Concentration contours on the z=10m plane for the base case. Each line is one order of magnitude difference in concentration in ppt.
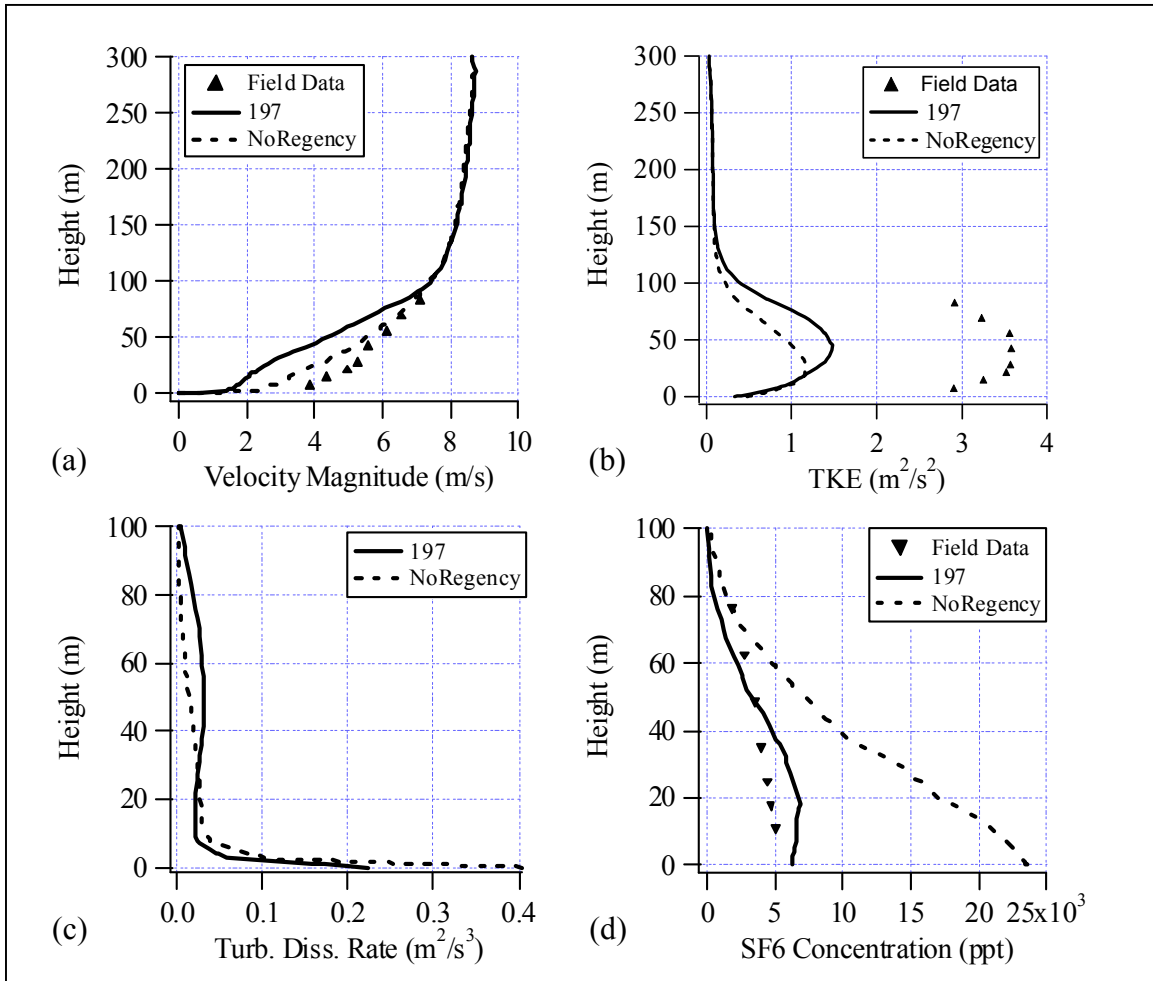
Figure 3-8. Vertical profiles of (a) velocity magnitude, (b) turbulent kinetic energy, (c) turbulent dissipation rate, and (d) SF_6 concentration at the crane position for the base case (197) and "no Regency" case.
The scale on (c) and (d) has been expanded to show detail.
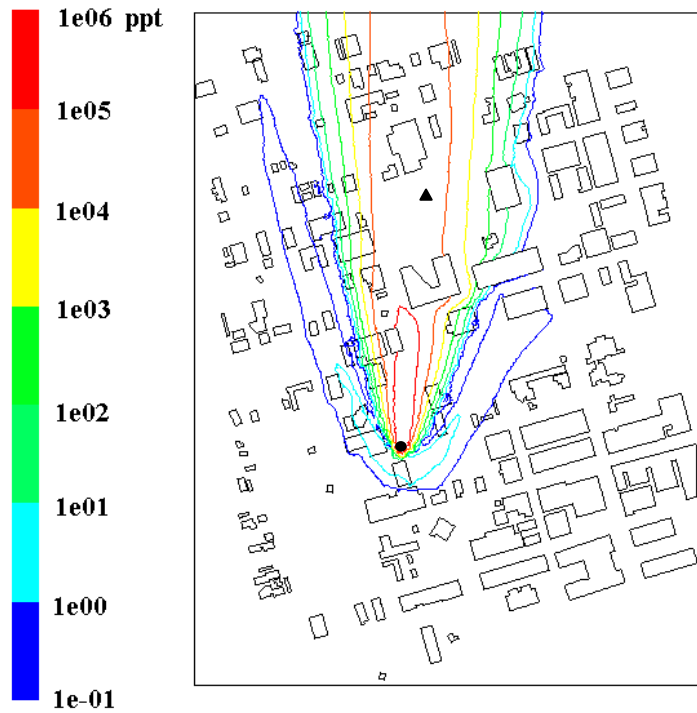
Figure 3-9. Concentration contours on the z=10m plane for the "no Regency" case.
Each line is one order of magnitude difference in concentration in ppt.
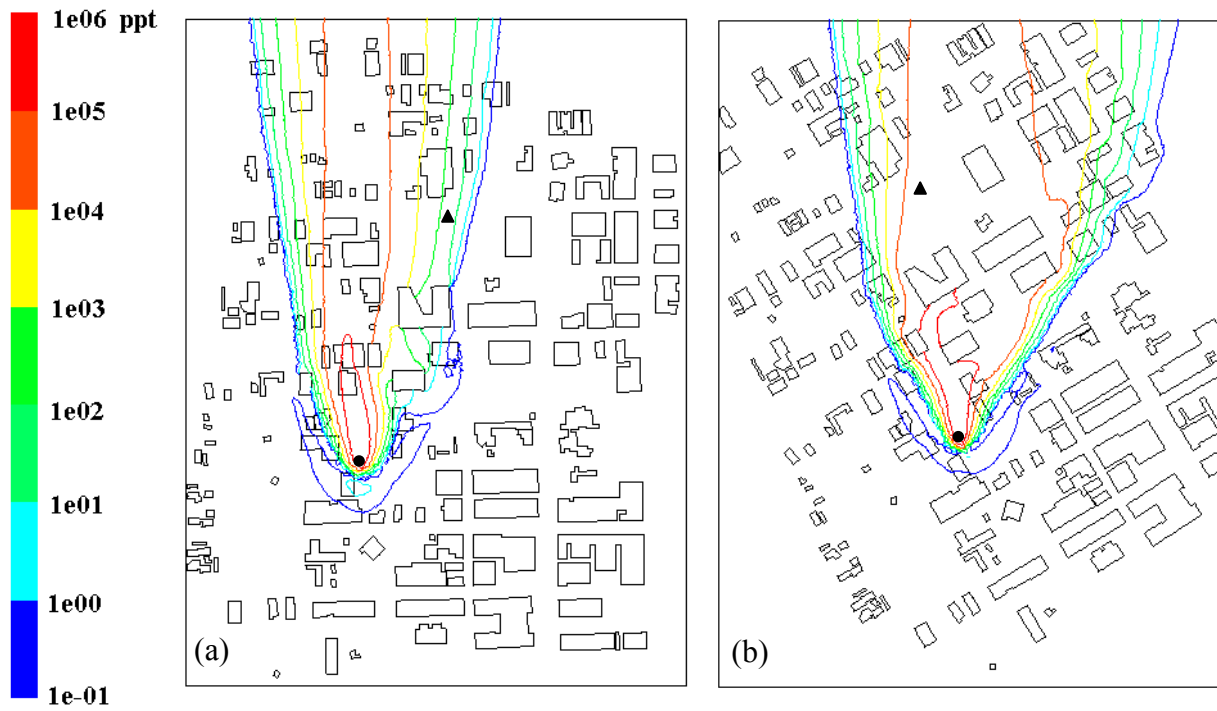
Figure 3-10. Concentration contours on the z=10m plane for the (a) 182-degree, and (b) 212-degree wind direction cases.
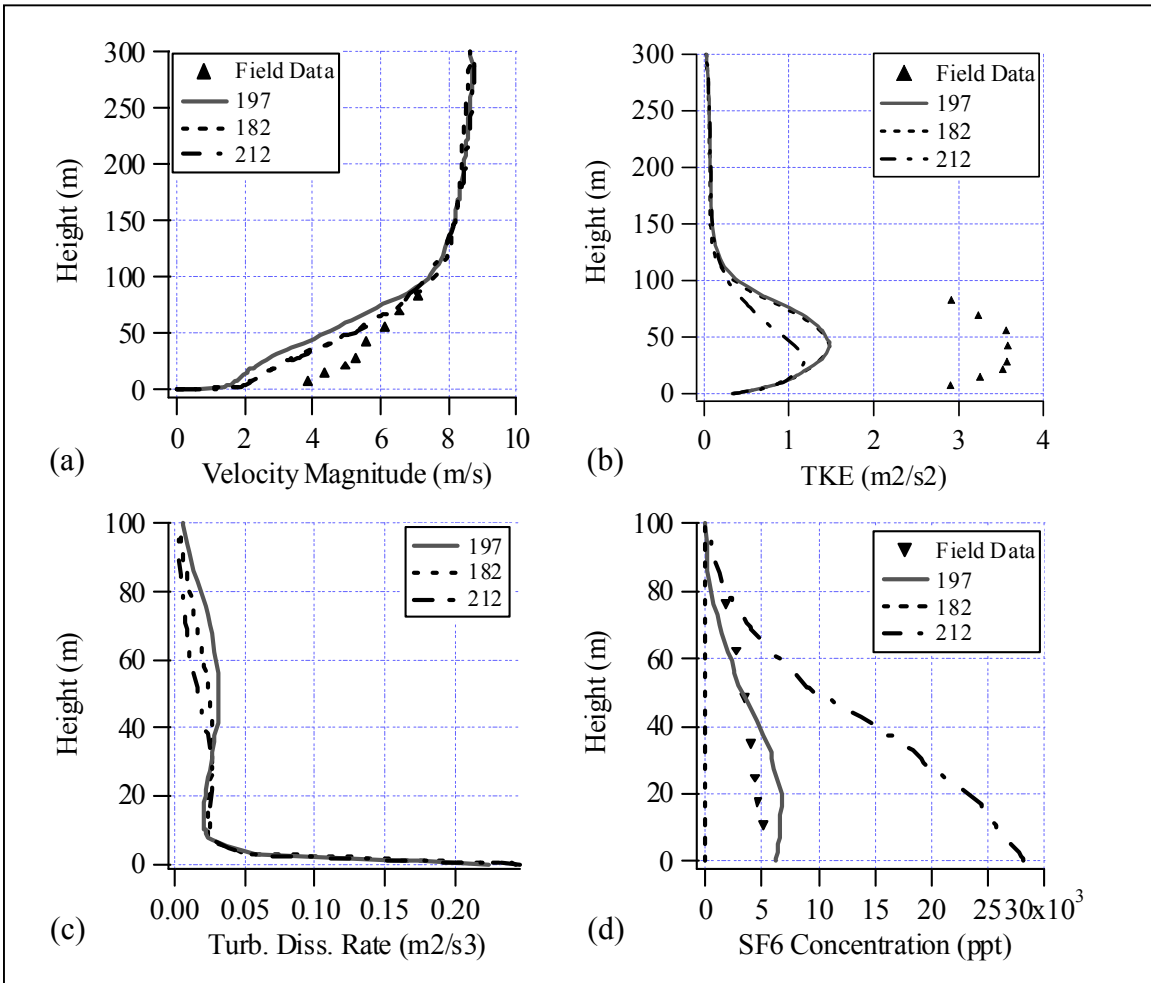
Figure 3-11. Vertical profiles of (a) velocity magnitude, (b) turbulent kinetic energy, (c) turbulent dissipation rate and (d) SF_6 concentration at the crane position for the base case (197) and two alternate wind direction cases (182 and 212). The scale on (c) and (d) has been expanded to show detail.
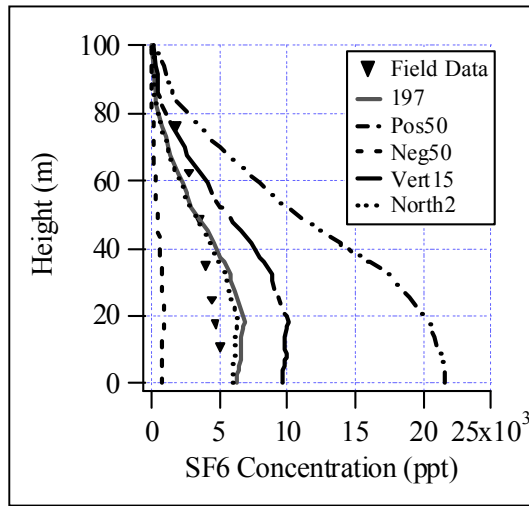
Figure 3-12. Concentration profiles for various source locations.
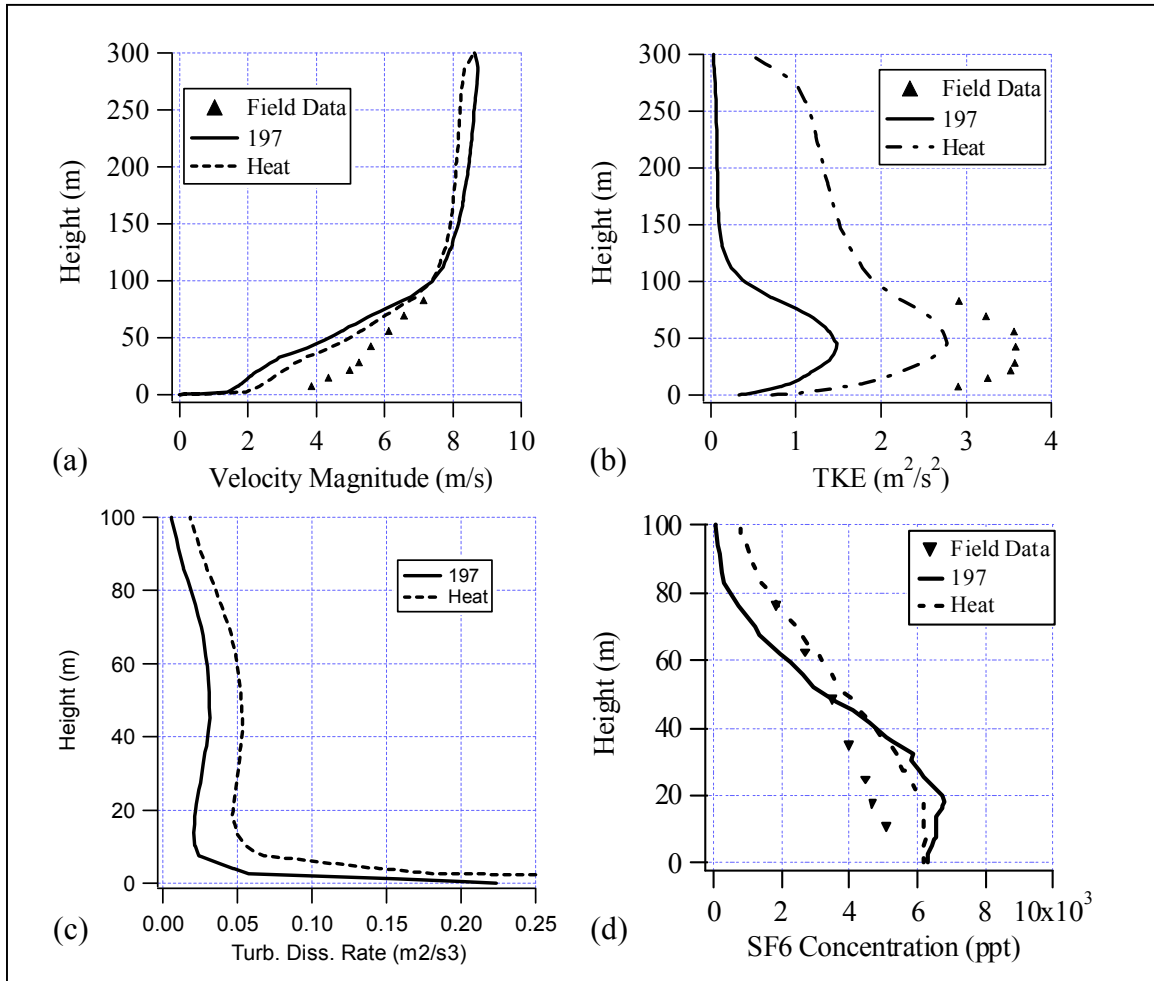
Figure 3-13. Vertical profiles of (a) velocity magnitude, (b) turbulent kinetic energy, (c) turbulent dissipation rate and (d) SF_6 concentration at the crane position for the base case (197) and the add heat case.
The scale on (c) and (d) have been expanded to show detail.

CHAPTER FOUR

SUMMARY AND CONCLUSIONS

The goal of this research was to investigate dispersion in an urban environment using a combination of experimental tracer and numerical fluid dynamic methods. This was accomplished through the two independent manuscripts presented in this thesis. An extensive field campaign was conducted in Oklahoma City, Oklahoma to collect a variety of measurements over a relatively large spatial extent. Vertical tracer profiles collected during this campaign were presented in Chapter Two. Then, a computational fluid dynamics (CFD) model was used to simulate a 10-minute field case and to investigate the mechanisms for dispersion in the urban landscape. The results of these modeling efforts were described in Chapter Three.

The Joint Urban 2003 field campaign, conducted during the summer of 2003, was an extensive field measurement program involving over 150 researchers from more than 20 institutions. Vertical profiles of tracer concentration at the Lawrence Livermore National Lab (LLNL) / Washington State University (WSU) crane site revealed that the plume is well-mixed by the mechanical mixing of the upwind urban landscape and the convective mixing from the heated urban surfaces. The complete set of vertical tracer profiles measured during this field study is presented as Figures A-1 through A-10 in the Appendix. Time series plots of the concentration, however, maintained the typical Gaussian shape. The variability in the concentrations measured at this site was due primarily to changes in wind direction, and did not exhibit a clear pattern with either wind speed or turbulent intensity.

Maximum concentration curves were developed using data from the NOAA Air Resources Laboratory Field Research Division (ARLFRD), Volpe, and WSU. Although a variety of averaging times were used throughout the experiment, the 5-minute averaged data

were used to include the WSU data. The piecewise curve developed using the 5-minute averaged data predicts a higher concentration at the source and was more shallow near the source than the Gaussian plume equation. Farther from the source, the slopes of the maximum concentration curve developed from the field data and the Gaussian plume equation were similar. Concentrations measured in the field were between two and three orders of magnitude greater than the Gaussian plume predictions. A computational fluid dynamics analysis was conducted to produce a maximum concentration curve that was fairly similar to the one derived from the field data.

A computational fluid dynamics analysis of a 10-minute study period from the Joint Urban 2003 field campaign was conducted and described in Chapter Three. The modeling domain was 900 meters wide, 1200 meters deep, and 300 meters tall. It included about 150 buildings and was meshed with 2,995,000 tetrahedral cells.

First, a grid uncertainty analysis was conducted to determine the accuracy of the computational results. The solution was computed with two coarse meshes, and a 6% grid convergence index was calculated for the tracer plume width at half-max. Celik and Karatekin (1997) describe the grid convergence index as a conservative estimate of the error band, and since 6% is within the error associated with field measurements, it was determined that the mesh resolution utilized in this study was sufficient. This grid uncertainty analysis utilized Richardson extrapolation (Richardson, 1910), which is the approved method for determining grid errors. Oftentimes, CFD studies of atmospheric dispersion do not address errors associated with the computational mesh. Other times, when this topic is mentioned, many groups choose to simply compute several mesh sizes and compare the solutions directly. This is not an acceptable

approach to characterizing the effects of the grid resolution, and it is hoped that future work in atmospheric flow and dispersion will adopt Richardson extrapolation.

Several modeling cases were considered to study the flow and dispersion in this urban landscape. The base case, an isothermal flow with the mean wind direction from the field study, resulted in tracer concentrations within 50% of the measured profile. The tallest obstruction in the plume path, the Regency Tower, was removed from the domain to observe the effects. Removing the Regency Tower resulted in a smaller gradient in the concentration profile at the crane site, and ground-level concentrations that were 5 times higher than the base case. This indicates that this tall structure served to mechanically mix the plume. Additionally, a flow field with thermal buoyancy due to building and ground surfaces with temperatures 10 degrees C hotter than the air temperature was computed. This resulted in an improved profile gradient and concentrations within 30% of the field measurements. Although the isothermal case predicted turbulent kinetic energy profiles with the correct shape, the magnitude of TKE along the profile was less than half of the observed values. Adding thermal buoyancy, however, significantly improved the turbulent kinetic energy profile. The modeled TKE peak for the buoyancy case was within 25% of the observations.

The Joint Urban 2003 field campaign has developed a high-quality dataset for studying urban transport and dispersion. The urban landscape is highly irregular, with buildings of varying shapes and sizes that result in unique flow and diffusion patterns. However, simple tools such as the maximum concentration curve developed here are necessary for a rapid assessment of dispersion by emergency personnel in the case of an emergency. More detailed work with computational fluid dynamics can continue to be utilized to understand the mechanisms for fluid flow and diffusion, as well as to contribute to the body of data available for developing

emergency response tools. Future work coupling field measurement campaigns with CFD modeling would benefit from a number of profiles of meteorology and turbulence for the depth of the urban boundary layer for use as inlet conditions for the modeling efforts. Additionally, as thermal buoyancy effects are considered, meta-data such as building surface materials, building and ground surface temperatures, and cloud cover would be a beneficial addition to the datasets of urban geometry.

REFERENCES

Celik, I., and O. Karatekin, 1997: Numerical experiments on application of Richardson extrapolation with nonuniform grids. *J. Fluids Eng.*, **119**, 584-590.

Richardson, L.F., 1910: The approximate arithmetical solution by finite differences of physical problems involving differential equations, with an application to the stresses in a masonry dam. *Philos. Trans. Roy. Soc. London*, **A 210**, 307-357.

APPENDIX
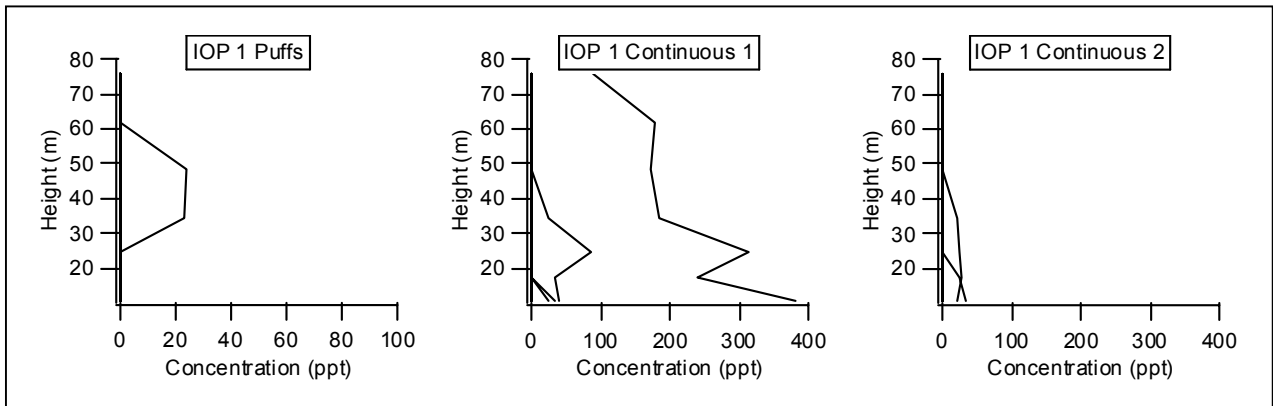
Figure A-1. Tracer concentration profiles from IOP 1.
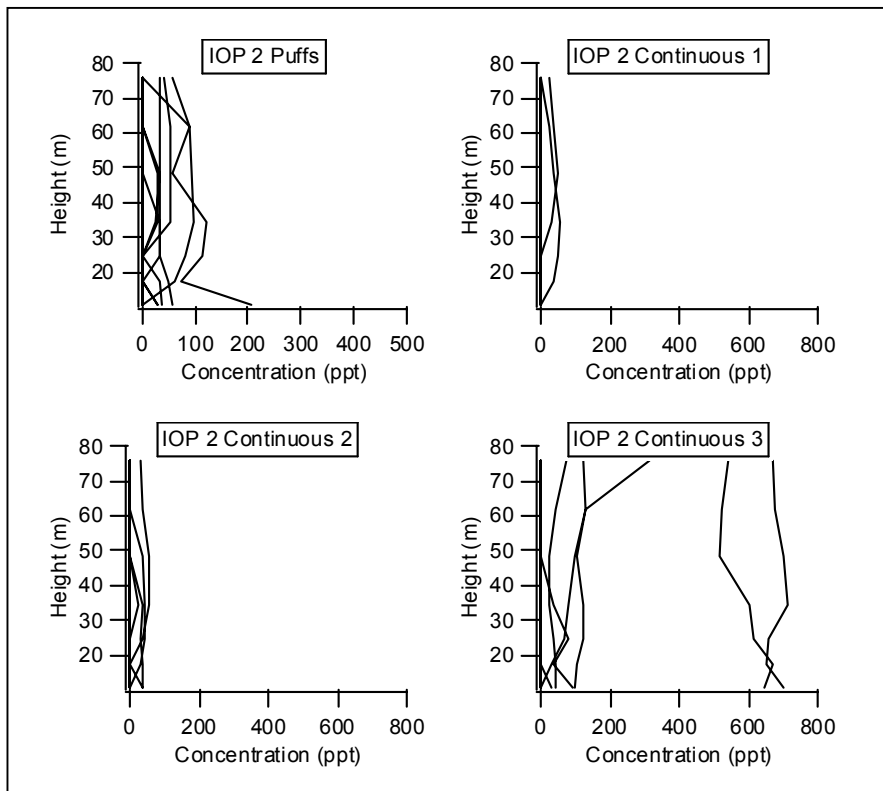
Figure A-2. Tracer concentration profiles from IOP 2.
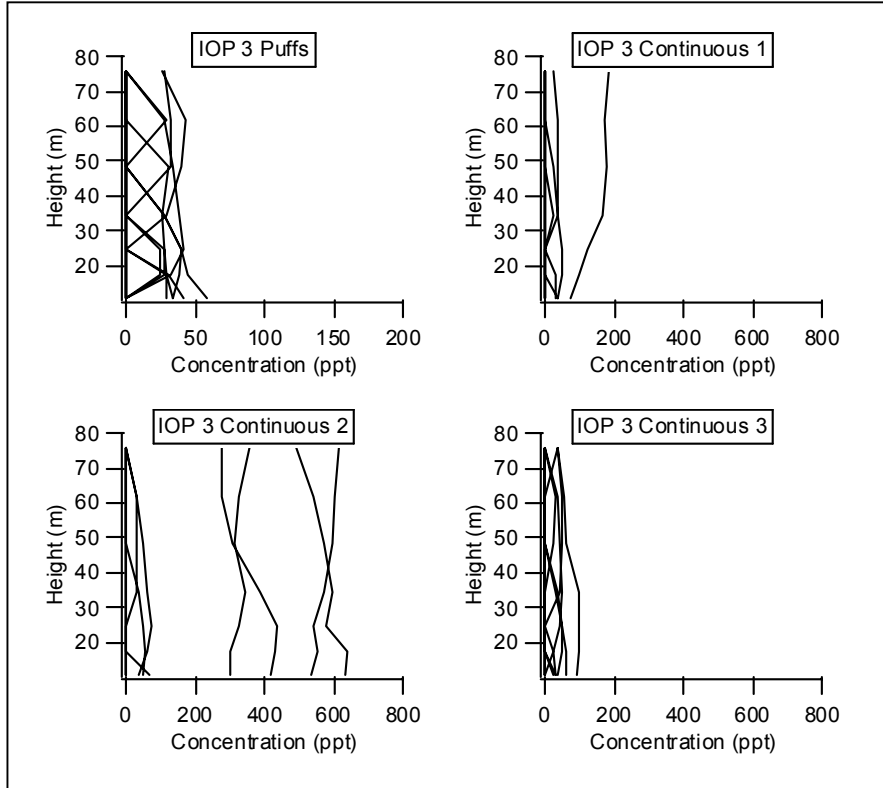
Figure A-3. Tracer concentration profiles from IOP 3.
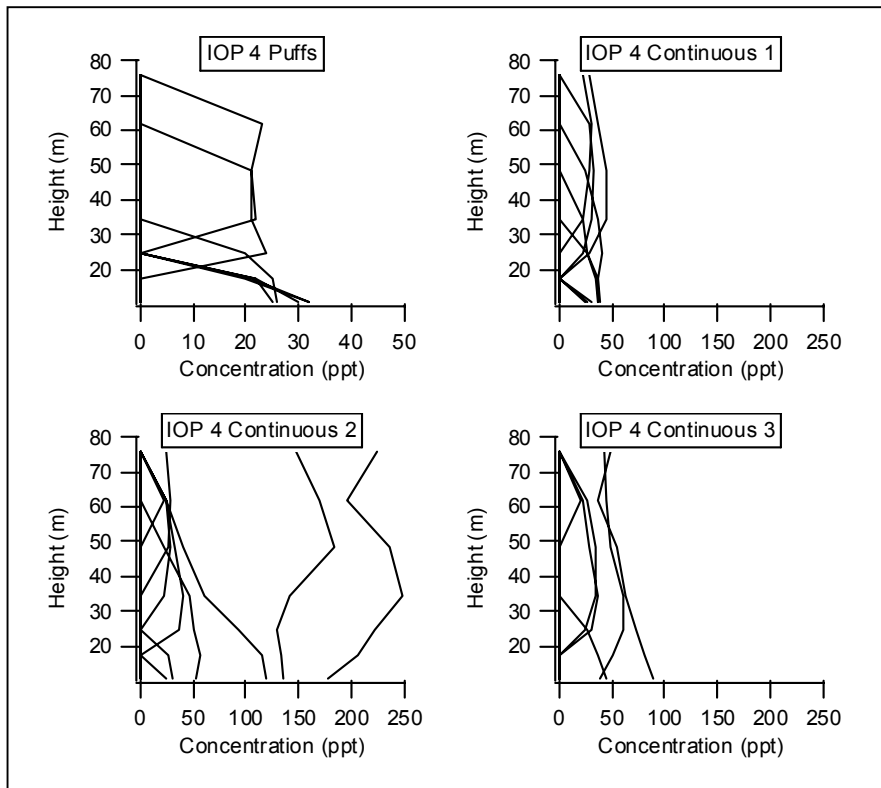

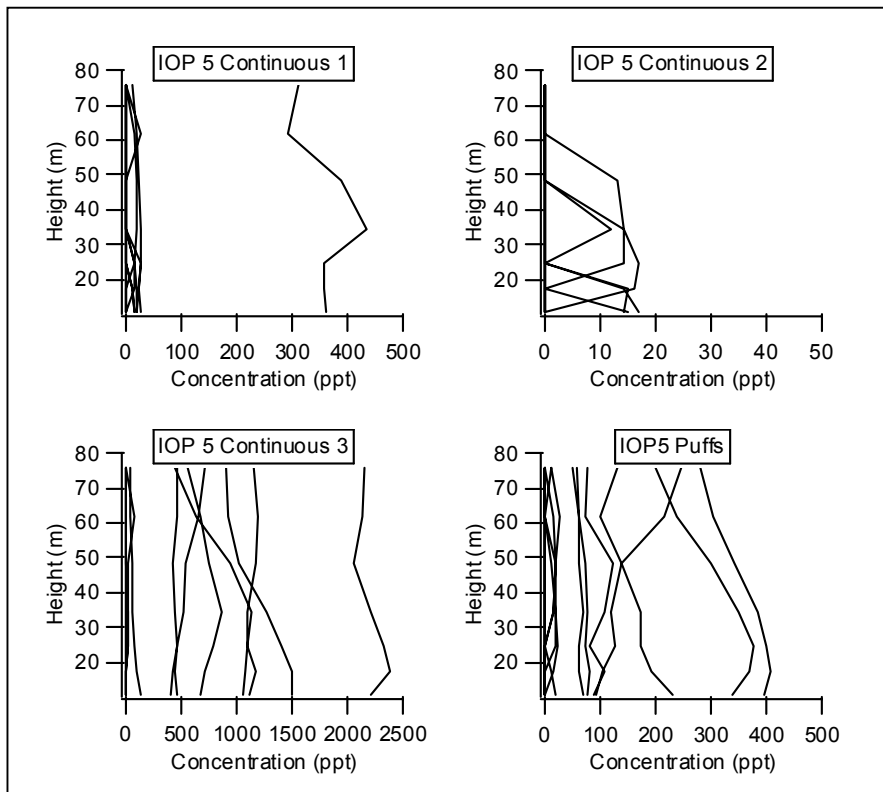Figure A-4. Tracer concentration profiles from IOP 4.

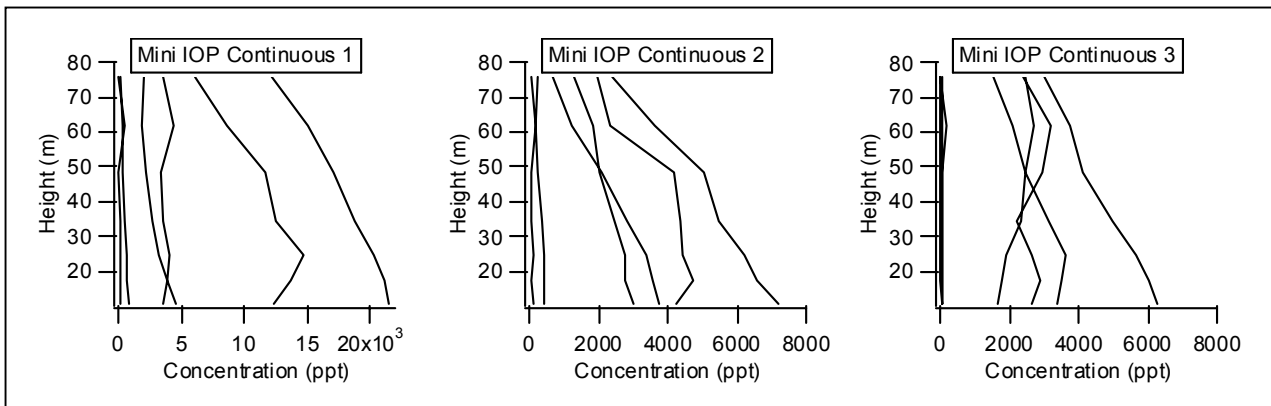Figure A-5. Tracer concentration profiles from IOP 5.

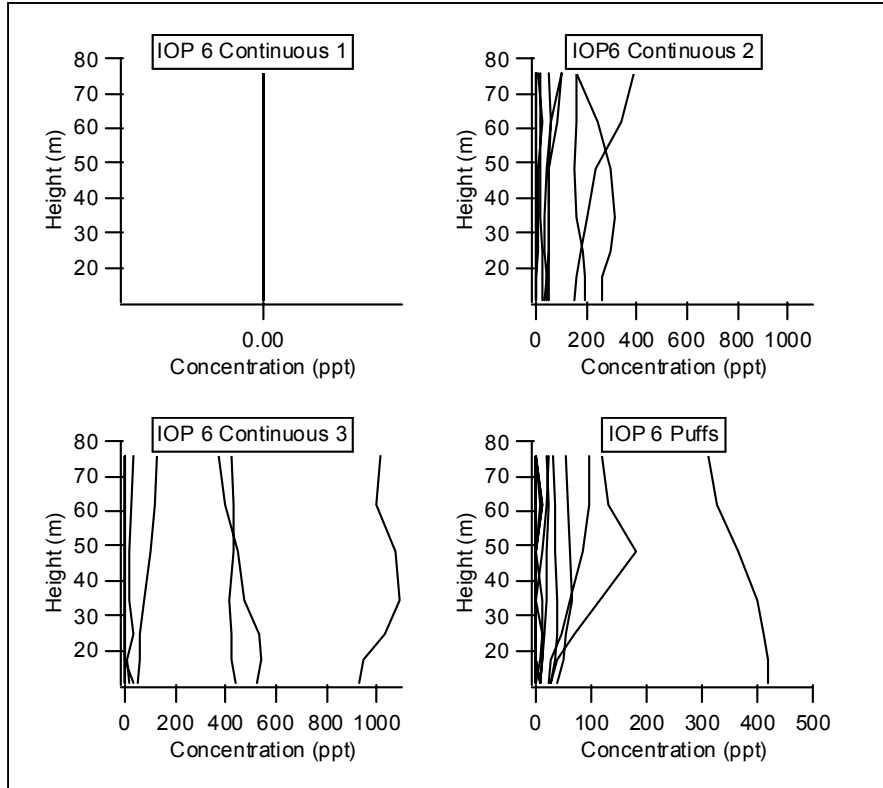Figure A-6. Tracer concentration profiles from the Mini IOP.

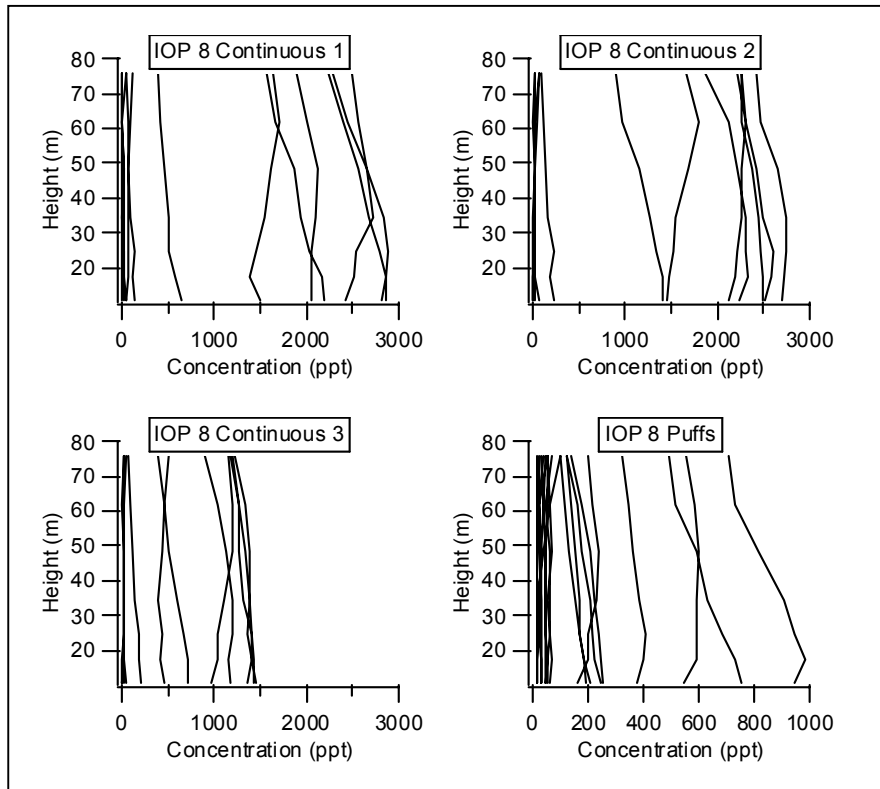Figure A-7. Tracer concentration profiles from IOP 6.

Figure A-8. Tracer concentration profiles from IOP 8.
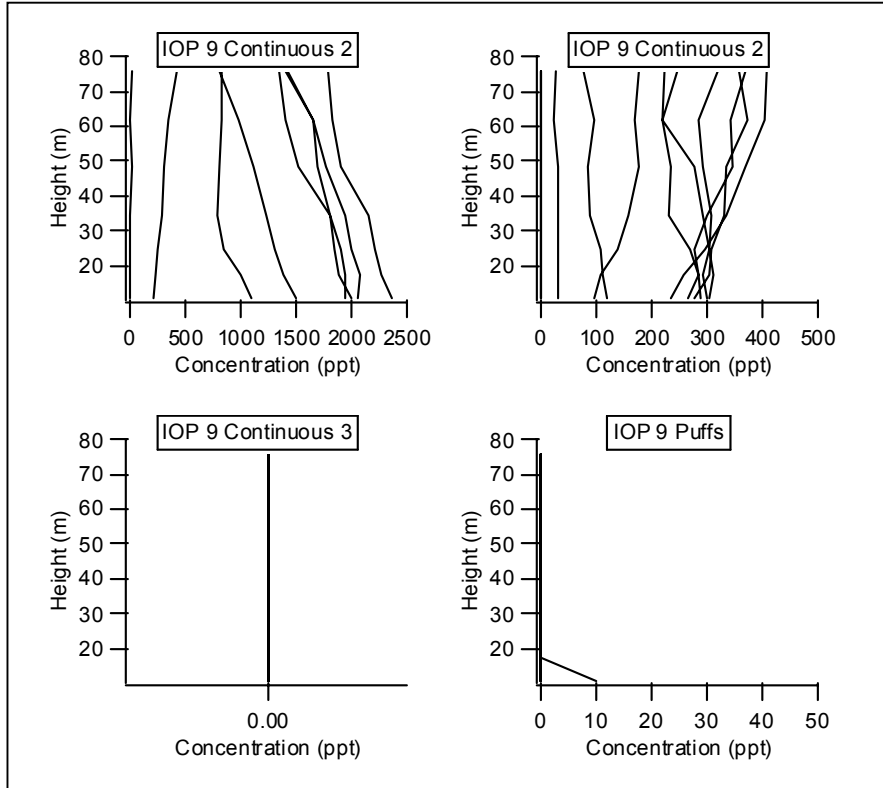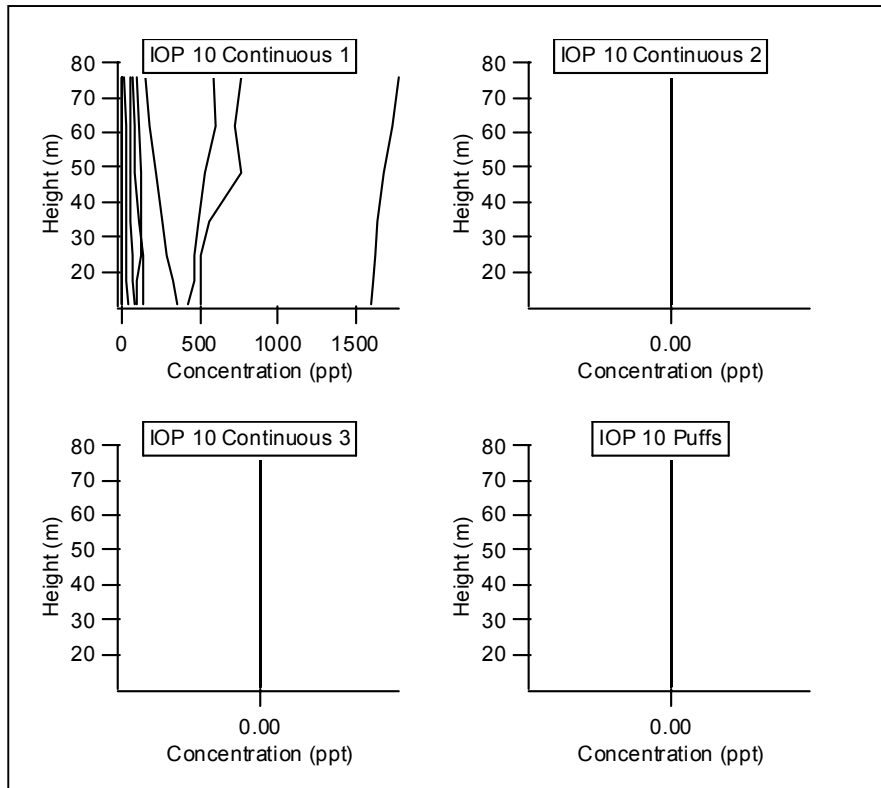
74

Figure A-9. Tracer concentration profiles from IOP 9.

Figure A-10. Tracer concentration profiles from IOP 10.